γ-Lyase in *Arabidopsis* and its implication in an alternative to the reverse trans-sulfuration pathway. *Plant Cell Physiol* **48**, 232–242.

40 Mamaeva DV, Morozova EA, Nikulin AD, Revtovich SV, Nikonov SV, Garber MB & Demidkina TV (2005) Structure of *Citrobacter freundii* L-methionine gamma-lyase. *Acta Crystallogr F Struct Biol Cryst Commun* **61**, 546–549.

41 Alston TA & Bright HJ (1983) Conversion of trifluoromethionine to a cross-linking agent by gamma-cystathionase. *Biochem Pharmacol* **32**, 947–950.

42 Clark CG, Alsmark UCM, Hofer M, Saito-Nakano Y, Ali V, Marion S, Mukherjee C, Bruchhaus I, Tannich E, Leippe M *et al.* (2007) Structure and content of the *Entamoeba histolytica* genome. *Adv Parasitol* **65**, 51–190.

43 Colombani F, Cherest H & de Robichon-Szulmajster H (1975) Biochemical and regulatory effects of methionine analogues in *Saccharomyces cerevisiae*. *J Bacteriol* **122**, 375–384.

44 Duewel H, Daub E, Robinson V & Honek JF (1997) Incorporation of trifluoromethionine into a phage lysozyme: implications and a new marker for use in protein 19F NMR. *Biochemistry* **36**, 3404–3416.

45 Soda K (1968) Microdetermination of D-amino acids and D-amino acid oxidase activity with 3-methyl-2-benzothiazolone hydrazone hydrochloride. *Anal Biochem* **25**, 228–235.

Supplementary material

The following supplementary material is available online:

Table S1. The oligonucleotide primers used in this study.

This material is available as part of the online article from http://www.blackwell-synergy.com

Please note: Blackwell Publishing are not responsible for the content or functionality of any supplementary materials supplied by the authors. Any queries (other than missing material) should be directed to the corresponding author for the article.

INFECTION AND IMMUNITY, Jan. 2008, p. 278–288
0019-9567/08/$08.00+0 doi:10.1128/IAI.00636-07

Vol. 76, No. 1

Autophagy during Proliferation and Encystation in the Protozoan Parasite *Entamoeba invadens*▽

Karina Picazarri, Kumiko Nakada-Tsukui, and Tomoyoshi Nozaki*

Department of Parasitology, Gunma University Graduate School of Medicine, Maebashi, Gunma 371-8511, Japan

Received 7 May 2007/Returned for modification 13 June 2007/Accepted 29 September 2007

Autophagy is one of the three systems responsible for the degradation of cytosolic proteins and organelles. Autophagy has been implicated in the stress response to starvation, antigen cross-presentation, the defense against invading bacteria and viruses, differentiation, and development. *Saccharomyces cerevisiae* Atg8 and its mammalian ortholog, LC3, play an essential role in autophagy. The intestinal protozoan parasite *Entamoeba histolytica* and a related reptilian species, *Entamoeba invadens*, possess the Atg8 conjugation system, consisting of Atg8, Atg4, Atg3, and Atg7, but lack the Atg5-to-Atg12 conjugation system. Immunofluorescence imaging revealed that polymorphic Atg8-associated structures emerged in the logarithmic growth phase and decreased in the stationary phase and also increased in the early phase of encystation in *E. invadens*. Immunoblot analysis showed that the increase in phosphatidylethanolamine-conjugated membrane-associated Atg8 was also accompanied by the emergence of Atg8-associated structures during the proliferation and differentiation mentioned above. Specific inhibitors of class I and III phosphatidylinositol 3-kinases simultaneously inhibited both the growth of trophozoites and autophagy and also both encystation and autophagy in *E. invadens*. These results suggest that the core machinery for autophagy is conserved and plays an important role during proliferation and differentiation in *Entamoeba*.

Amoebiasis is a diarrheal disease caused by the protozoan parasite *Entamoeba histolytica* and affects approximately 50 million inhabitants of areas where the disease is endemic, resulting in an estimated 40,000 to 110,000 deaths annually (61). Its transmission occurs through the ingestion of food or water contaminated with infective cysts (33). Although encystation is an essential fundamental process required for the transmission of the disease, little is known about biochemical and cell biological changes or the regulation of gene expression that occurs during this process except in some cases (5, 7, 10–12, 47, 57). In the reptilian *Entamoeba* species *E. invadens*, 18 genes, including those for ubiquitin 48, gene 122 (47), chitinases 1 and 2 (7, 57), two isoforms of chitin synthases (chs-1 and chs-2) (5), and the cyst-specific lectins called Jacob (7) and Jessie (5, 57), were differentially expressed at different stages of encystation. However, various fundamental events that occur during encystation, which allow drastic changes in cellular compositions and organelle structures, remain largely uncharacterized except for the involvement of proteasomes (12). Recently, a transcriptome of *E. histolytica* clinical isolates which identified some novel *E. invadens* stage-specific genes has been documented (10).

Autophagy is a cellular process highly conserved in eukaryotes which permits the degradation of long-lived proteins and damaged or unnecessary organelles (24). Autophagy has been implicated in various biological processes, including the stress response to carbon and nitrogen starvation; antigen cross-presentation; the defense against invading bacteria, viruses, and other intracellular pathogens; differentiation; and development (15, 25, 28, 30, 38, 49, 51). Autophagosome formation is initiated by the emergence of an isolation membrane in the cytosol, called the preautophagosomal structure (PAS) (36, 50, 58). The PAS elongates and expands to form the autophagosome membranes (19, 25, 36) that enclose cytosolic components and organelles, including mitochondria and endosomes (14, 18, 45). Autophagosomes subsequently fuse to lysosomes, leading to the degradation of sequestered organelles and materials (15, 25). In *Saccharomyces cerevisiae*, 16 autophagy-related (*Atg*) genes that encode components essential for autophagy were identified (21). Autophagosome formation is regulated by two related ubiquitin-like (UBL) systems in both yeast and mammals (25, 54). The first UBL system allows the conjugation of Atg12 to Atg5. After the Atg12-to-Atg5 conjugation, these proteins form a complex with Atg16 (22), and this complex acts upstream of the second conjugation system. In the second conjugation system, where Atg8 is a major anchoring molecule, Atg4 protease (54) exposes the terminal glycine of Atg8 (36). Atg8 is subsequently activated by the E1 enzyme Atg7 (54) and transferred to Atg3, an E2-like enzyme, which conjugates Atg8 to phosphatidylethanolamine (PE) (17). Atg4 also participates in Atg8 deconjugation, which is essential for the fusion of autophagosomes with lysosomes/vacuoles (2, 4, 20, 54, 62). Among the components involved in these conjugation systems, Atg8 has been considered to be an authentic marker for autophagosomes because lipid-anchored Atg8 remains attached to the inner membrane of autophagosomes until it is degraded by lysosomal hydrolases after the fusion with lysosomes (36).

The biological importance of autophagy has been demonstrated both in vitro and in vivo with various organisms (9, 16, 23, 29, 44, 63). In *Caenorhabditis elegans*, the inhibition of *Atg1*, *Atg6*, *Atg7*, *Atg8*, and *Atg10* by RNA interference resulted in a defect in the organism's morphogenesis to the dauer stage,

* Corresponding author. Mailing address: Department of Parasitology, Gunma University Graduate School of Medicine, 3-39-22 Showa-machi, Maebashi, Gunma 371-8511, Japan. Phone: 81 27 220 8020. Fax: 81 27 220 8025. E-mail: nozaki@med.gunma-u.ac.jp.

▽ Published ahead of print on 8 October 2007.

when the organism takes a dormant form between the L2 and L3 larval stages under conditions of high population density, reduced levels of nutrients, or increased temperature. Under such conditions, development ceases so that the organism can survive for an extended period (34). In the social ameba *Dictyostelium discoideum*, Atg8 plays a role in survival and spore formation. During starvation, *D. discoideum* develops a multicellular form that functions like a spore reservoir. A mutant lacking *Atg5* or *Atg7* was unable to produce viable, mature spores, and autophagosome formation was abolished under conditions of starvation (41). A *Leishmania major vps4* mutant which showed a defect in endosomal sorting and the fusion of Atg8 autophagosomes with lysosomes failed to differentiate from a diving procyclic promastigote into the infective metacyclic form (4).

In this study, we show by a genome-wide survey that *E. histolytica* and the related reptilian species *Entamoeba dispar* and *E. invadens* possess genes involved in the Atg8 conjugation but not those of the Atg5-to-Atg12 conjugation pathway. Furthermore, we demonstrate, by immunoblot and immunofluorescence assays, that autophagy occurs in two independent phases—the logarithmic growth phase and the early phase of encystation—in the life cycle of *E. invadens*.

MATERIALS AND METHODS

Bacteria, chemicals, and reagents. The *Escherichia coli* DH5α and BL21(DE3) strains were purchased from Life Technologies (Tokyo, Japan) and Invitrogen (Tokyo, Japan), respectively. All chemicals were of analytical grade and were purchased from Sigma-Aldrich (Tokyo, Japan) or Wako (Tokyo, Japan) unless otherwise stated.

***E. invadens* culture and encystation.** Trophozoites of the *E. invadens* IP-1 strain were cultured axenically in BI-S-33 medium at 26°C. To induce encystation, 2-week-old *E. invadens* cultures were passaged in 47% LG medium lacking glucose (47) at approximately 6×10^5 cells/ml. Amoebae were collected at various time points, and the formation of cysts was assessed by virtue of the resistance to 0.05% Sarkosyl using 0.22% trypan blue to selectively stain dead cells. Cysts were also verified by cyst wall staining by incubating amoebae with calcofluor white (fluorescent brightener 28; Sigma-Aldrich) at room temperature.

Genome-wide survey of genes involved in autophagy in *Entamoeba*. *S. cerevisiae* Atg proteins were obtained from the NCBI nonredundant protein database (http://www.ncbi.nlm.nih.gov/) and used as queries to search for orthologs in the *E. histolytica*, *E. dispar*, and *E. invadens* genome databases (http://www.tigr.org/tdb/e2k1/eha1, http://www.sanger.ac.uk/Projects/E_histolytica/, http://www.sanger.ac.uk/Projects/E_dispar/, and http://www.sanger.ac.uk/Projects/E_invadens). Possible orthologs were further analyzed with the blastp algorithm (http://www.ncbi.nlm.nih.gov/BLAST/) against the nonredundant database at NCBI to find the closest homologs in other organisms.

Production of recombinant EhAtg8 and antiserum against EhAtg8. Standard techniques were used for routine DNA manipulation, subcloning, and plasmid construction as previously described (46). The protein coding region of *E. histolytica Atg8a* (EhAtg8a) (locus tag XP_649165) was amplified using oligonucleotide primers (5′-CATCCCGGGATGGAATCACAACCAAAACTT-3′ and 5′-AGACTCGAGTTAATTTCCAAAGACAGATTC-3′) and the *E. histolytica* cDNA library (39) by PCR. The parameters used for the PCR were an initial step of denaturation at 94°C for 2 min, followed by 30 cycles of denaturation at 94°C for 15 s, annealing at 55°C for 30 s, and an extension at 65°C for 1 min. A final step of denaturation at 95°C for 9 s, annealing at 60°C for 9 s, and an extension at 95°C for 9 s was used to remove primer dimers. A 408-bp PCR fragment was cloned in the SmaI-XhoI site of the pGEX-6P-2 expression vector (GE Healthcare Bioscience, Tokyo, Japan) to produce pGST-EhAtg8. The pGST-EhAtg8 plasmid was introduced into the *E. coli* BL21(DE3) strain. The expression of the glutathione *S*-transferase (GST)-EhAtg8 recombinant protein was induced, and cell lysate was produced according to the instructions of the manufacturer. The GST tag at the amino terminus of the recombinant GST-EhAtg8 construct was cleaved by Precision protease (GE Healthcare Bioscience) and removed by GSTrap (GE Healthcare Bioscience). The recombinant EhAtg8 protein was further purified by Mono Q anion-exchange chromatography on an AKTA Explorer chromatograph (GE Healthcare Bioscience). Rabbit antiserum against EhAtg8 was commercially produced (Kitayama Rabesu, Nagano, Japan).

Cell fractionation. Amoebae were harvested, washed with phosphate-buffered saline containing 2% glucose, and resuspended in a homogenization buffer (50 mM Tris, pH 7.5; 250 mM sucrose; 50 mM NaCl; and 1.34 mM *trans*-epoxysuccinyl-L-leucylamido-[4-guanidino butane]). The amoebae were homogenized with 80 to 300 strokes (depending on the percentage of cysts) in a glass homogenizer and centrifuged at 400 × *g* for 5 min at 4°C to remove unbroken cells. The supernatant was further centrifuged at 100,000 × *g* for 1 h to separate a high-speed pellet from the supernatant, both of which were subjected to immunoblot analysis.

Immunoblot analysis. To differentiate unmodified and PE-conjugated Atg8, sodium dodecyl sulfate-polyacrylamide gel electrophoresis (SDS-PAGE) was conducted using 13.5% separating gel containing 6 M urea, as previously described (20). Approximately 5 μg of lysates or fractions were separated by denaturing SDS-PAGE and transferred to nitrocellulose membranes. After the membranes were blocked with 5% skim milk, they were incubated with anti-EhAtg8 or anti-EhNifS (1) antibody (1/1,000 dilution) for 1 h. After being washed, the membranes were incubated with anti-rabbit immunoglobulin G (IgG) alkaline phosphatase-conjugated antibody (Jackson Laboratories, Bar Harbor, ME) or horseradish peroxidase-conjugated antibody (Amersham Bioscience, Piscataway, NJ) for 1 h. Proteins were visualized with an alkaline phosphatase conjugate substrate kit (Bio-Rad, Hercules, CA) or by chemiluminescence with the Immobilon Western substrate (Millipore Corporation, Billerica, MA). The intensity of the bands visualized by chemiluminescence was detected on a Lumi-Imager F1 workstation (Roche Applied Science, Tokyo, Japan) with the LumiAnalyst software (Roche Applied Science) and further analyzed with ImageJ.

Indirect immunofluorescence assay. Trophozoites and cysts were fixed in 3.7% paraformaldehyde in phosphate-buffered saline for 10 min at room temperature, washed, and permeabilized with 0.2% saponin for 10 min. Then, the cells were incubated with anti-EhAtg8 antibody (1/1,000 dilution) for 1 h at room temperature and subsequently incubated with anti-rabbit IgG Alexa Flour 488 antibody (Invitrogen) for 1 h at room temperature. Finally, the cells were washed, mounted on a glass slide, and examined under a confocal laser scanning microscope (LSM 510 Meta; Carl Zeiss, Thornwood, NY). The images were further analyzed with LSM 510 software.

Nucleotide and protein sequence accession numbers. The nucleotide and protein sequences reported in this paper have been submitted to the DDBJ with accession numbers AB326955 (*E. invadens Atg8* [Ei*Atg8*]) and AB326956 (Ei*Atg3*).

RESULTS AND DISCUSSION

One of the two UBL systems is conserved in *E. histolytica*. In yeast and mammals, the biogenesis of autophagosomes is regulated by two UBL systems (25, 54). The *E. histolytica* genome (HM-1:IMSS [8]) apparently encodes only one of the two UBL systems (Table 1). We identified genes encoding two Atg8 proteins (designated EhAtg8a and EhAtg8b), four Atg4 proteins (designated EhAtg4a to EhAtg4d), one Atg7 protein, and one Atg3 protein. The two EhAtg8 proteins showed 96% identity to each other. EhAtg8a and EhAtg8b showed 31 to 33, 25 to 27, and 28 to 30% identity to bee *Apis mellifera* Atg8a, yeast Atg8, and γ-aminobutyric acid receptor-like 2 (Gabarapl2) from amphioxus *Branchiostoma belcheri tsingtauense*, respectively, the last of which was shown to be expressed during the early embryo and larval development phases (26).

EhAtg4a to EhAtg4d showed 22 to 26% identity to yeast and mammalian Atg4. Atg4 belongs to a new class of cysteine proteases (CPs) (20), which differ in function and structure from other CPs, such as the papain, HAUSP, UCH-L3, and Ulp1 families (52). EhAtg4s lack a prodomain typically present in most amoebic CPs. In addition, the active-site cysteines that are well conserved among cathepsin L-like CPs, e.g., CP1, CP2, and CP5, are not aligned with those in these Atg4s (data not

TABLE 1. The Atg8 conjugation system is conserved in *E. histolytica*

S. cerevisiae protein name	Accession no.[a]	Putative EhAtg	*E. histolytica* locus tag/accession no.[b]	E value against *S. cerevisiae* ortholog	Best hit		Best hit against mammals	
					Organism, locus tag or accession no. (protein name)[a]	E value	Organism, locus tag or accession no. (protein name)[a]	E value
Atg8	P38182	Atg8a	XP_649165/337.m00048	4e−6	*A. mellifera*, XP_001120069 (Atg8a)	7e−8	*Pan troglodytes*, XP_511114 (Gabarapl2)	5e−7
		Atg8b	XP_649940/258.m00050	2e−4	*A. mellifera*, XP_001120069 (Atg8a)	4e−7	*Macaca mulatta*, XP_001104154 (Gabarapl2)	1e−6
Atg4	P53867	Atg4a	XP_653798/72.m00167	6e−12	*Strongylocentrotus purpuratus*, XP_786847 (autophagy-related 4D)	7e−17	*Canis familiaris*, XP_851977 (CP Apg4b)	2e−13
		Atg4b	XP_656724/8.m00420	5e−12	*Trypanosoma brucei*, XP_829686 (peptidase)	1e−14	*Pan troglodytes*, XP_001145426 (CP Atg4a)	4e−11
		Atg4c	XP_652043/134.m00147	5e−8	*Trypanosoma cruzi*, XP_813094 (Atg4)	4e−6	*Bos taurus*, XP_873804 (cysteine endopeptidase AUTLlike 4)	1e−5
		Atg4d	XP_651386/168.m00116	6e−6	*Bos taurus*, Q6PZ05 (CP Atg4a)	1e−11	*Bos taurus*, Q6PZ05 (CP Atg4a)	4e−11
Atg7	P38862	Atg7	XP_654007/65.m00164	1e−104	*D. discoideum*, XP_645809 (autophagy protein 7)	6e−108	*M. musculus*, NP_083111 (autophagy-related protein 7)	2e−102
Atg3	P40344	Atg3	XP_654705/46.m00258	5e−29	*Strongylocentrotus purpuratus*, XP_001175772 (similar to MGC80121 protein)	3e−37	*Rattus norvegicus*, Q6AZ50 (autophagy-related protein 3)	2e−26
Atg5	Q12380		XP_651022/186.m00113	6.3e−1	*Anopheles gambiae*, BAC82595 (reverse transcriptase)	1e−8	*Canis familiaris*, XP_851237 (LINE-1 reverse transcriptase)	7e−2
Atg10	Q07879		XP_650961/190.m00098	4.5e−1	*Gibberella zeae*, XP_390739 (hypothetical protein)	1.7	*Canis familiaris*, XP_534421 (similar to chromodomain helicase DNA binding protein 6)	2.8
Atg12	P38316		XP_650304/229.m00072	6e−2	*Ostreococcus tauri*, CAL57467 (kinesin, putative)	2e−3	*Canis familiaris*, XP_848707 (similar to myosin, heavy polypeptide 7, cardiac muscle)	4e−3
Atg16	Q03818		XP_654748/45.m00158	3e−5	*Schizosaccharomyces pombe*, BAA06454 (SMC4, structural maintenance of chr4)	1e−80	*Canis familiaris*, XP_535848 (structural maintenance of chromosomes 4-like 1 protein)	1e−78

[a] NCBI database numbers.
[b] NCBI locus tag/accession number from the *E. histolytica* genome database at The Institute for Genomic Research.

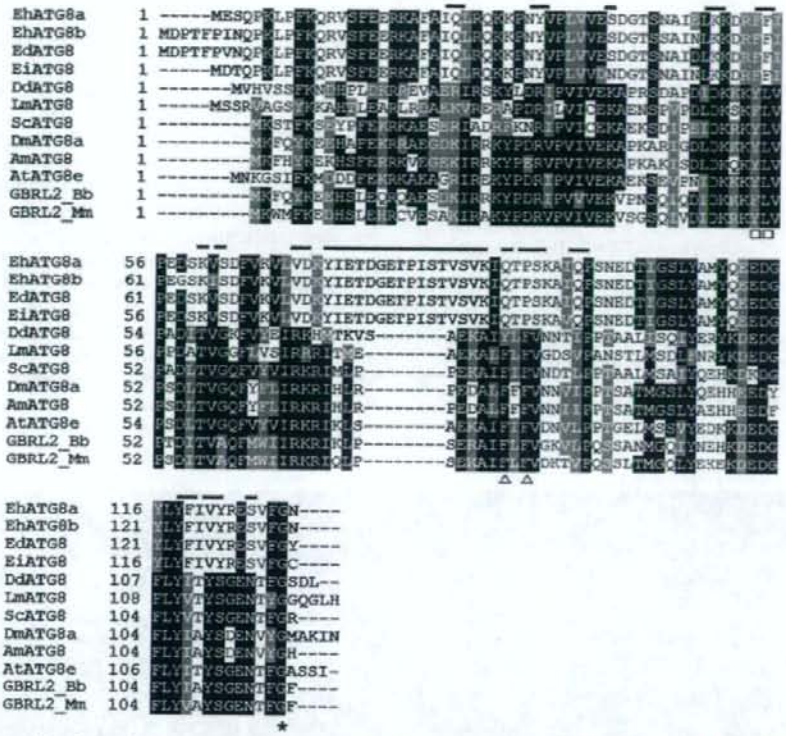

FIG. 1. Alignment of Atg8 protein sequences from three *Entamoeba* species and other organisms. Clustal W (http://www.ch.embnet.org/software/ClustalW.html) and BoxShade 3.21 (http://www.ch.embnet.org/software/BOX_form.html) were used to produce the alignment. Conserved amino acid residues are shown with a black background, and conserved substitutions are shown with a gray background. Gaps are shown by dashes. The asterisk under the alignment indicates the consensus glycine that is conjugated to PE. Residues implicated in binding to Atg4 and autophagy activity are depicted with triangles and squares under the alignment, respectively. *Entamoeba*-specific residues are overlined. Sequences used in the alignment were those for EdAtg8 (*E. dispar* genome accession no. AANV01003233), EiAtg8 (accession no. AANW01005912, nt 44 to 433), EhAtg8a (locus tag XP_649165), EhAtg8b (locus tag XP_649940), DdAtg8 (*Dictyostelium discoideum*, locus tag XP_637841), LmAtg8.1 (*Leishmania major*, EMBL accession no. CAJ07266), ScAtg8 (*Saccharomyces cerevisiae*, Swiss-Prot accession no. P38182), DmAtg8a (*Drosophila melanogaster*, locus tag NP_727447), AmAtg8 (*Apis mellifera*, locus tag XP_001120069), AtAtg8e (*Arabidopsis thaliana*, locus tag NP_182042), GBRL2_Bb (Gabarapl2 from *Branchiostoma belcheri*, accession no. AAO45172), and GBRL2_Mm (Gabarapl2 from *Mus musculus*, EMBL accession no. BAB22217).

shown). These EhAtg4s were previously reported as "autophagins 1 to 4," which are members of the C54 cysteine endopeptidase family (6). In yeast, only one isoform of Atg4 has been reported (53, 55), while *Homo sapiens* apparently possesses four Atg4 homologs (52). The putative Atg3 and Atg7 homologs (EhAtg3 and EhAtg7) showed 31 to 47% and 34 to 38% identities to yeast and mammalian counterparts, respectively. On the other hand, *E. histolytica* apparently lacks genes encoding Atg5, Atg10, Atg12, and Atg16 (Table 1).

The presence of the Atg8 conjugation system and the concomitant absence of the Atg5-to-Atg12 conjugation pathway were also reported for both the free-living social amoeba *Dictyostelium* (41) and the parasitic protist *Leishmania* (60). These data may indicate that the Atg8 conjugation system is evolutionarily older than the Atg5-to-Atg12 conjugation system and that the former represents minimal machinery required for autophagy. As shown below, the Atg8 conjugation system is apparently sufficient for autophagosome biogenesis, at least in these protists (4, 41).

Conservation of the Atg8 conjugation pathway in related *Entamoeba* species, namely, *E. dispar* and *E. invadens*. *E. dispar* is the commensal nonpathogenic species for mammals, while *E. invadens* is the invasive reptilian species and a primary model of encystation. Although the *E. dispar* and *E. invadens* genomes have not been completed, we identified two *Atg8* genes (locus tags AANV01003233 and AANV01014404), one *Atg4* gene (AANV01002875), two *Atg7* genes (AANV01000460 and AANV01009354), and one *Atg3* gene (AANV01000567) in the *E. dispar* database, while only one *Atg8* gene (AANW0100 5912, nucleotides [nt] 44 to 433), one *Atg4* gene (AANW0101 0411, nt 5 to 1166; the gene likely contains an intron, but the carboxyl terminus of the protein is incomplete), and one *Atg3* gene (AANW01009890, nt 424 to 1226 in a complementary strand) were found in the *E. invadens* genome database (data

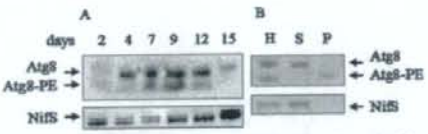

FIG. 2. Immunoblot analysis of Atg8 in *E. invadens*. (A) Immunoblot analysis of Atg8 in *E. invadens* trophozoites cultured in a normal proliferation medium. *E. invadens* trophozoites were cultivated in BI-S medium at the indicated times (days 2 to 15), and whole lysates were electrophoresed by SDS-PAGE, blotted, and reacted with anti-EhAtg8 (top panel) or a control antibody against EhNifS (1) (bottom panel). A representative blot from three independent experiments is shown. (B) Cell fractionation of Atg8. A whole lysate produced by mechanical homogenization of trophozoites, harvested 1 week after the initiation of the culture at a cell density of ~5×10^4 cells/ml, was separated into the supernatant and pellet fractions by centrifugation at 100,000 × *g* and subjected to immunoblot analysis as described above. Lane H, a whole homogenate; lane S or P, a supernatant or a pellet after centrifugation at 100,000 × *g* centrifugation, respectively.

not shown). We were unable to identify an *Atg7* ortholog in the *E. invadens* genome, likely due to incomplete sequencing of the genome. Comparison of EiAtg8 and *E. dispar* Atg8 (EdAtg8) to EhAtg8a and EhAtg8b showed that EiAtg8 is 99% and 95% identical to EhAtg8a and EhAtg8b and that EdAtg8 is 98% and 96% identical to EhAtg8a and EhAtg8b, respectively. The high degree of conservation in *E. invadens* is remarkable considering that this species has shown itself to be largely divergent from *E. histolytica* and *E. dispar*, as indicated by the significant differences in codon usage and G-C content between *E. invadens* and *E. histolytica*/*E. dispar* (40).

Features of *Entamoeba* Atg8. Amino acid comparisons by using Clustal W (Fig. 1) highlighted a number of unique features of *Entamoeba* Atg8. Phe77 and Phe79 (numbered as for *Saccharomyces cerevisiae* Atg8), implicated in the interaction with Atg4 in yeast (2), are not conserved in Atg8 proteins from *Entamoeba* species but are well conserved in *Leishmania*, *Arabidopsis* spp., and mammals. Neither are other important

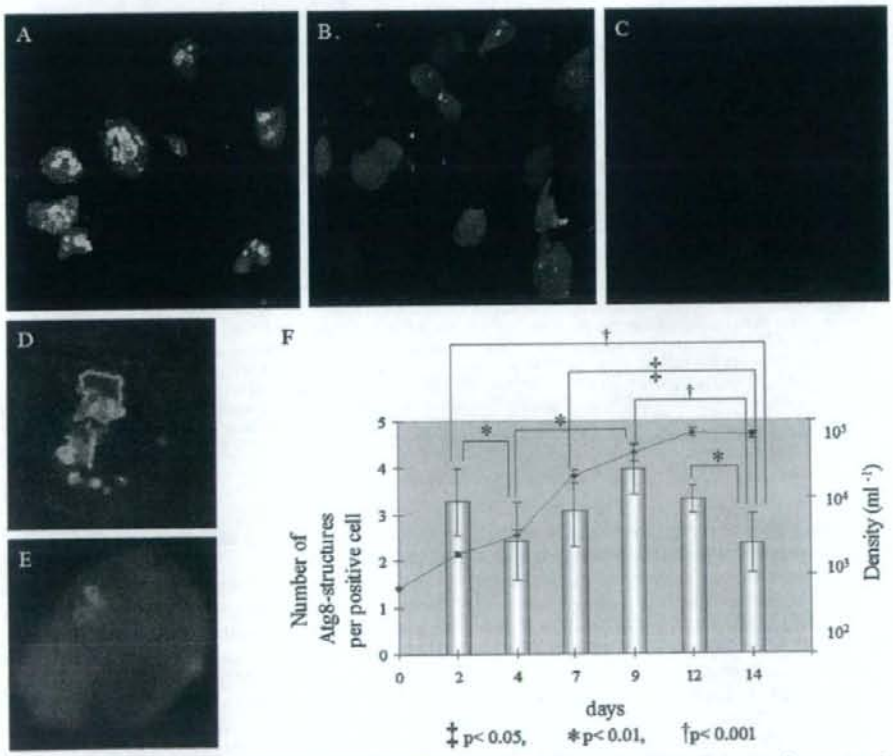

FIG. 3. Immunofluorescence imaging of autophagy in proliferating trophozoites of *E. invadens*. (A to C) Immunofluorescence images of Atg8 in proliferating *E. invadens*. Maximum-projection images of 8 to 10 *E. invadens* trophozoites of 1 (A)- and 2 (B)-week-old cultures reacted with anti-EhAtg8 antibody under low magnification are shown. One-week-old culture was also reacted with preimmune serum (C). (D to E) Confocal images under high magnification of a representative slice of a single typical trophozoite harvested at 1 week (D) or 2 weeks (E). (F) Growth kinetics of *E. invadens* trophozoites and autophagosome formation in the normal proliferation medium. Cell density was measured in triplicate, and the means and standard deviations are shown with diamonds connected by a solid line. Trophozoites in proliferation were assayed by immunofluorescence as previously described; the average numbers of Atg8-positive structures per positive cell were counted and are shown by the bars. Approximately 30 to 40 cells were examined at each time point. Pairwise comparisons between each time point, with statistical significance (*P* value of <0.001, <0.01, or <0.05), are also indicated.

residues involved in the autophagy activity in yeast (Tyr49 and Leu50) (2) conserved in *Entamoeba* Atg8. A number of other residues totally conserved in Atg8 proteins from other organisms are not conserved in *Entamoeba*; these residues are distributed throughout the entire protein (Fig. 1).

All *Entamoeba* Atg8s share a unique 16-amino acid insertion (e.g., amino acids 72 to 88 of EhAtg8a; YIETDGETPISTVS VK). Based on the crystal structure of Atg8 from yeast, this region is located 1 to 5 residues upstream of the Atg4 recognition site (Phe-X-Phe, which is absent in *Entamoeba* Atg8) and thus predicted to be exposed on the surface of the molecule and possibly interacts with other proteins. We also examined the nucleotide sequence of this region of all *Entamoeba Atg8* genes and excluded the possibility that this region corresponds to an intron by reverse transcriptase PCR of cDNA (data not shown). EhAtg8b has an extra 5-amino-acid amino-terminal extension (MDPTF), which is also present in EdAtg8 but missing in EiAtg8. Interestingly, the overall identities of EdAtg8 and EiAtg8 to EhAtg8a or EhAtg8b are not consistent with the fact that EiAtg8 lacks the 5-amino-acid amino-terminal extension present in EhAtg8b but that EdAtg8 possesses it. It is unlikely that the lack of this amino-terminal extension in EiAtg8 is due to an incomplete genome database because the open reading frame of Ei*Atg8* is not located at the end of the contig AANW01005912 (nt 44 to 433 of the total length of 1,166 nt).

Immunoblot analysis of Atg8 in *E. invadens*. In order to verify if autophagy occurs in *Entamoeba* and, if it does, to identify growth phases and stages where autophagy plays a role, immunoblot analysis of *E. invadens* trophozoites cultured in a regular proliferation medium with anti-EhAtg8 antibody was conducted (Fig. 2). Two bands with molecular masses of approximately 15.0 and 14.5 kDa were observed (Fig. 2A). Dramatic changes in both the total amount of Atg8 and the proportions of the two forms were found during 2 weeks of culture. The intensity of both the 15.0- and 14.5-kDa Atg8 bands increased in the mid- and late-logarithmic growth phases (days 4 to 12) and peaked at day 9, while it decreased at days 2 and 15. The ratios of the intensity of the 15.0-kDa band to that of the 14.5-kDa band were 2.4, 1.4, 1.1, and 2.2 at days 4, 7, 9, and 12, respectively, based on chemiluminescence measurements of these bands (data not shown). These data correlate well with the results of the immunofluorescence study (Fig. 3) (see below).

Cell fractionation followed by immunoblot assay (Fig. 2B) showed that 15.0-kDa Atg8 was fractionated almost exclusively to the soluble, likely cytosolic, fraction but that the 14.5-kDa Atg8 was found in the pellet fraction centrifuged at 100,000 × *g*. On the basis of the results of a number of other studies (17, 20), we concluded that the top band corresponds to the cytosolic, nonconjugated Atg8 protein and that the bottom band corresponds to the membrane-associated PE-conjugated Atg8 protein.

Immunofluorescence imaging of Atg8 in proliferating *E. invadens* trophozoites. Immunofluorescence analysis revealed remarkable changes in the Atg8-associated autophagosome-like structures in *E. invadens* trophozoites in both the logarithmic and stationary growth phases. Microscopic images of cultures at representative time points—1 and 2 weeks—under low magnification showed homogeneous Atg8 staining in each population, but remarkable differences in intensity were observed between 1- and 2-week-old cultures (Fig. 3A and B). In order to further investigate the observed growth-phase-dependent synthesis and degradation of autophagosomes, we quantified the number of Atg8-associated structures, examined under high magnification, during the exponential to stationary growth phases (Fig. 3D to F). The average number of Atg8-associated autophagosome-like structures (see below for morphological categories) peaked at 9 days in the BI-S-33 proliferation medium. Although the number of Atg8-associated structures was more than three per cell at day 2, the structures were mainly dot-like or tiny vesicles (data not shown), which is consistent with the repression of *Atg8* demonstrated by immunoblot analysis.

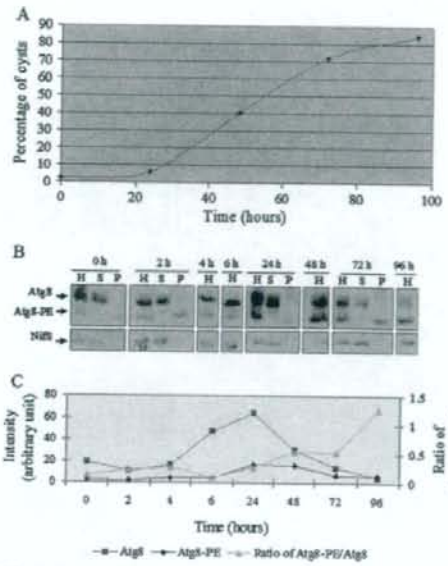

FIG. 4. Immunoblot analysis of Atg8 in *E. invadens* during encystation. (A) Kinetics of encystation. The percentages of the amoebae resistant to 0.05% Sarkosyl during encystation are shown. (B) *E. invadens* trophozoites were harvested at the indicated times, lysed, fractionated as described for Fig. 2B, and subjected to immunoblot analysis by using anti-EhAtg8 (top panel) or anti-EhNifS (bottom panel) antibody, followed by chemiluminescence detection. Lanes: H, whole homogenate; S and P, supernatant and pellet, respectively, after centrifugation at 100,000 × *g*. (C) Densitometric measurements from immunoblots developed by chemiluminescence. Only representative quantitations from three immunoblots which exhibited similar kinetics are shown.

Expression and membrane recruitment of Atg8 change during encystation in *E. invadens*. Autophagy has recently been implicated in differentiation during nutrient deprivation in organisms such as *C. elegans*, *D. discoideum*, and *Leishmania* (4, 34, 41, 60). Although it has recently been demonstrated that encystation-specific genes could be identified in *E. histolytica* clinical isolates (10), in vitro encystation of both *E. histolytica* clinical isolates and laboratory strains has not been accomplished. To further investigate if autophagy is induced during encystation, we exploited the encystation of *E. invadens* with

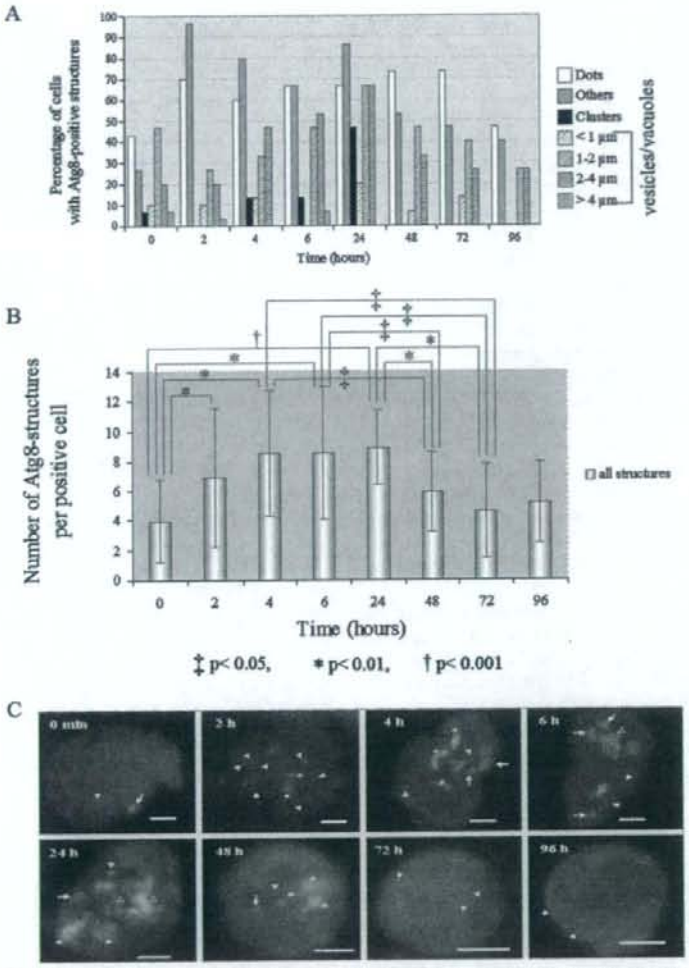

FIG. 5. Kinetics of Atg8-positive autophagosome-like structures during encystation by immunofluorescence assays. (A) Percentages of amoebae containing categorized Atg8-positive structures during encystation are shown. The categories are cytosolic; dot-like; vesicles/vacuoles with diameters of <1.0 μm, 1.0 to 2.0 μm, 2.0 to 4.0 μm, and >4.0 μm; other structures; and clusters. (B) Average numbers of Atg8 structures, as categorized above, per positive amoeba. Approximately 30 to 40 cells were examined at each time point, and means and standard deviations are shown. Pairwise comparisons between each time point, with statistical significance (P value of <0.001, <0.01, or <0.05), are also indicated. Representative results of three independent experiments are shown in panels A and B. (C) Subcellular localization of Atg8 during encystation. Representative images of a maximum projection of approximately 20 slices taken at 1-μm intervals on the z axis at each time point are shown. Filled arrowheads, open arrowheads, arrows, and asterisks indicate Atg8-positive dot-like structures, clusters, vesicles/vacuoles, and other structures, respectively. Bars = 5 μm.

2-week-old cultures as an inoculum into the 47% LG medium lacking glucose. Under these conditions, we accomplished up to 80 to 93% encystation within 96 h, based on Sarkosyl resistance (Fig. 4A). We also verified that the kinetics of the increment of Sarkosyl-resistant amoebae and that of the calcofluor-stained amoebae were almost indistinguishable (data not shown). Although encystation is usually induced in trophozoites using 2- to 3-day-old cultures (12) or 7-day-old cultures in the logarithmic growth phase (32), we used 2-week-old cultures as an inoculum. As described above, the amount of Atg8 protein and the number of membrane-associated Atg8-positive structures were significantly lower in the 2-week-old cultures than in the 2- to 7-day-old cultures, and thus the kinetics of Atg8 synthesis and the formation of the Atg8-positive structures during encystation could ideally be monitored by using 2-week-old cultures.

Amoebae were harvested at various time points, and Atg8 was first examined by immunoblotting and quantitated as de-

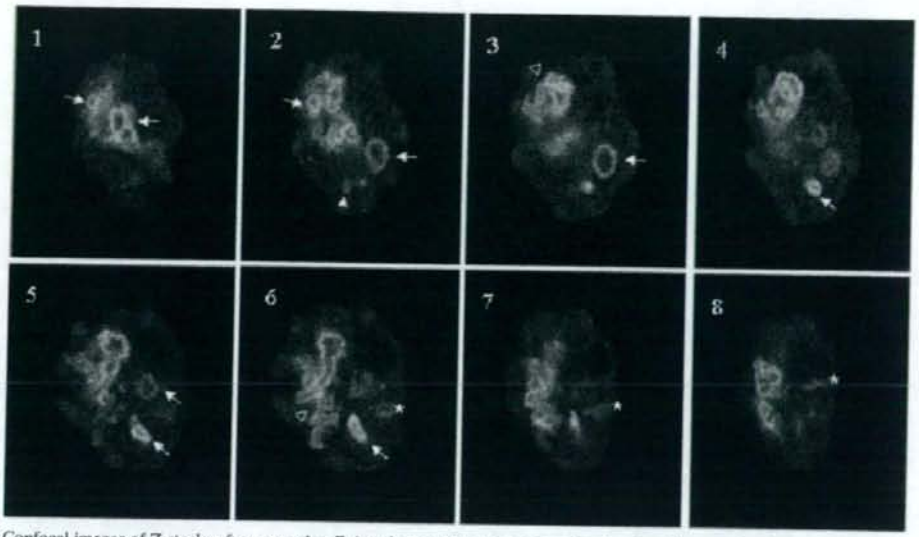

FIG. 6. Confocal images of Z stacks of an encysting *E. invadens* trophozoite. *E. invadens* trophozoites were incubated in 47% LG medium for 24 h and analyzed by immunofluorescence assay with anti-EhAtg8 antibody and Alexa 488-conjugated anti-rabbit IgG antibody. Eight slices of a representative trophozoite were captured at 1-μm intervals on the *z* axis and are shown from the bottom to the top. A filled arrowhead, an open arrowhead, arrows, and asterisks indicate representative Atg8-positive dot-like structures, clusters, vesicles/vacuoles, and other structures, respectively.

scribed above (Fig. 4B and C). The amount of unmodified Atg8 was reduced as early as 2 h after the amoebae were transferred to the encystation medium. Concomitantly, the amount of PE-modified Atg8 increased and peaked at 24 to 48 h. The total amount of Atg8, estimated by chemiluminescence assay, changed during encystation. The ratio of PE-conjugated Atg8 to unmodified Atg8 also changed significantly. The ratio of Atg8-PE to unmodified Atg8 also increased in a course of encystation (e.g., 0.09 or 1.26 at 6 or 96 h, respectively). These data are similar to the observation about the formation of autophagosomes under starvation conditions in other organisms (19). Interestingly, at 24 h after the induction of encystation, the production of PE-modified Atg8 reached a plateau, while only 7% of the trophozoites differentiated into cysts, as evaluated by detergent resistance (Fig. 4A) and calcofluor staining (data not shown). Thus, the emergence of PE-conjugated Atg8 precedes encystation. To verify that autophagy really occurs in encysting cells, we examined the presence of Atg8-associated structures in detergent-resistant cysts after Sarkosyl treatment. Although we were unable to simultaneously examine cyst markers and Atg8 due to technical problems (i.e., calcofluor cannot be used in an immunofluorescence assay), these data are consistent with the premise that cluster formation increases as encystation proceeds.

Immunofluorescence assay reveals dramatic changes in the autophagosome-like structures during encystation. Immunofluorescence imaging of encysting *E. invadens* cultivated in 47% LG medium showed that both the percentage of amoeba-containing structures and the number of structures per amoeba increased during encystation (Fig. 5). Representative stacks of Atg8 structures at 24 h after the induction of *E. invadens* encystation are shown in Fig. 6. We morphologically categorized the Atg8-associated structures into several groups: "dots" (containing no luminal region); "vesicles/vacuoles" of <1, 1 to 2, 2 to 4, or >4 μm in diameter (containing a luminal region surrounded by Atg8-positive structures); "others" (including linear or thread-like structures); and "clusters" (containing multiple dots, vesicles, vacuoles, and other structures) (Fig. 5A and C). Atg8-positive dots and other structures, including linear and diffuse/amorphous structures, were observed in almost all cells in the population. As early as 2 h after the induction of encystation, both the percentages of cells containing the Atg8-positive dot-like and other structures and the numbers of these structures per cell started to increase, peaked at 24 h, and then gradually decreased from 24 to 96 h. Both the numbers and sizes of the vesicular/vacuolar structures increased from 4 to 24 h; e.g., at 24 h, approximately 65% of the amoebae contained large Atg8-positive vesicles/vacuoles 2 to 4 μm in diameter. The Atg8-positive clusters emerged mainly after 24 h. Concomitant with the emergence of the cluster structures, the percentage of cysts started to increase, suggesting that cluster formation may coincide with the initiation of morphological and biochemical encystation.

The dot structures observed in this study were similar to those typically referred to as PAS (Fig. 5C), which correspond to a perivacuolar site containing lipids and early autophagy proteins such as Atg8/LC3 (27). PAS undergoes elongation and originate double membranes called isolation membranes (36, 58). It was reported that in yeast, the diameter of the autophagosomes ranges from 0.3 to 0.9 μm (58), while it usually ranges up to 1.5 μm in mammals (e.g., embryonic stem cells, embryonic fibroblasts, hepatocytes, and pancreatic acinar

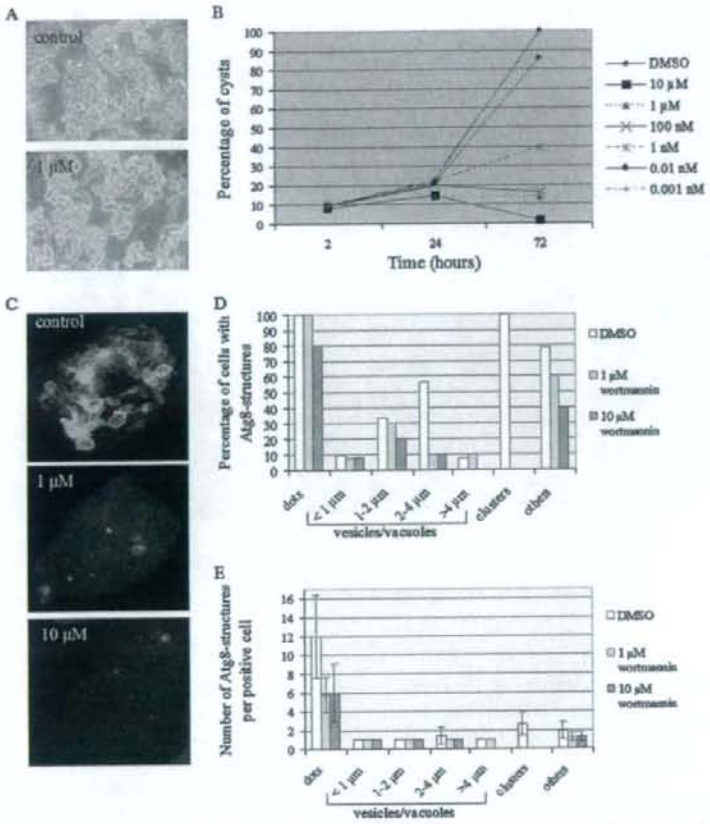

FIG. 7. Inhibition of encystation and the formation of autophagosomes by wortmannin in *E. invadens*. (A) Micrographs of amoebae at 72 h after induction of encystation with or without wortmannin. *E. invadens* trophozoites were incubated in 47% LG medium and supplemented with dimethyl sulfoxide (DMSO) (control) or 1 μM wortmannin. (B) Percentages of cysts after 2, 24, or 72 h of incubation in the encystation medium with various concentrations of wortmannin. The results of a representative set of three independent experiments are shown. (C) Immunofluorescence images of EiAtg8-positive structures in cells not treated or treated with 1 or 10 μM wortmannin in the encystation medium for 2 days. Representative images of the maximum projection of approximately 20 slices taken at 1-μm intervals on the *z* axis are shown. (D) Percentages of amoebae containing categorized Atg8-positive structures during encystation in the presence of 1 or 10 μm wortmannin are shown. (E) Average numbers of Atg8-positive structures per positive amoeba in the absence or presence of 1 or 10 μM wortmannin. Representative results of three independent experiments are shown.

cells) (35). Therefore, the sizes of the Atg8-associated autophagosome-like structures in *Entamoeba* shown in the present study are unprecedented, except for the 5- to 10-μm autophagosomes containing group A streptococci, *Mycobacterium tuberculosis*, and *Toxoplasma* (3, 13, 37). Under nonstarvation conditions, we found predominantly 1- to 2-μm Atg8-positive vesicles/vacuoles in proliferating trophozoites, suggesting that vesicles/vacuoles of this size represent autophagosomes constitutively formed under normal conditions. This is similar to what was reported for mammalian cells where autophagy was constitutively active or suppressed in response to specific hormones (58).

PI 3-kinase inhibitors abolish proliferation, encystation, and the formation of autophagosomes in *E. invadens*. The proliferation of trophozoites was severely affected by wortmannin, a well-known fungal phosphatidylinositol (PI) 3-kinase inhibitor, which was shown to inhibit autophagy in yeast, mammals, and *Leishmania* (4, 27). The growth of trophozoites cultivated in the BI-S-33 medium containing 1 μM wortmannin for 1 week was impaired by >90% (data not shown). Immunofluorescence analysis showed that the average number of the Atg8-associated structures decreased by 25% in trophozoites treated with the inhibitor (data not shown).

We next examined the effects of the inhibition of PI 3-kinase by wortmannin or 3-methyladenine during encystation. Wortmannin at ≥100 nM completely inhibited encystation as measured by Sarkosyl resistance at 72 h (Fig. 7B). Concomitantly, 1 μM of wortmannin also inhibited the rounding and agglutination of parasites, which was normally observed during encystation (Fig. 7A). These data are consistent with previous

findings (31). The immunofluorescence assay showed that the formation of Atg8-associated structures was abolished by wortmannin (Fig. 7C to E). Both the percentage of positive cells and the number of Atg8-associated clusters and vesicles/vacuoles, particularly those 2 to 4 μm and >4 μm in diameter, per cell significantly decreased after wortmannin treatment (Fig. 7D and E). Although the percentage of cells containing dots did not change, the average number of these punctate structures, which presumably correspond to PAS, was reduced by 50% ($P < 0.05$). The simultaneous dose-dependent inhibition of encystation and the autophagosome formation are consistent with the involvement of PI 3-kinase in the biogenesis, most likely by fusion and/or aggregation, of autophagosomes in *Entamoeba* and with the fact that autophagy plays an important role in encystation. Both encystation and the formation of Atg8-associated structures were also simultaneously inhibited by 3-methyladenine, although the effective concentrations were >100-fold higher than those of wortmannin (data not shown). It was previously shown that wortmannin inhibits PI 3-kinases with a 50% inhibitory concentration of ~10 nM and that 3-methyladenine is less potent than wortmannin (its 50% inhibitory concentration is ~10^6-fold higher than that of wortmannin) (27). Wortmannin and 3-methyladenine inhibit the class III PI 3-kinases, including Vps34 (42), which forms PI 3-kinase complex I (58), an essential component of PAS (36), by competition with ATP binding (27). *E. histolytica* apparently possesses at least three—*Vps34* (locus tag XP_656932), *Vps15* (XP_652375), and *Apg6/Beciclin 1* (XP_656050)—of the four components necessary to form the PI 3-kinase complex, while the remaining component, *Apg14*, is absent from its genome. However, since proliferation, autophagy, and survival were shown to be regulated by Tor kinase, a class I and III PI 3-kinase (25, 27, 48, 56), the possibility that the defect of proliferation or encystation is not causally connected but simply coincides with the inhibition of autophagy cannot be excluded.

Significance of autophagy in *Entamoeba*. The presence of autophagosome-like structures in proliferating trophozoites of both *E. invadens* and *E. histolytica* (data not shown but described elsewhere) suggests a housekeeping role for autophagy in this group of protists. The remarkable increase in the formation of autophagosomes in the mid- to late logarithmic growth phase and their repression in the stationary phase are consistent with the hypothesis that autophagy likely plays a role in proliferation but not in survival during starvation. The involvement of autophagy during proliferation was also suggested for mouse T cells (43).

In addition to the role of autophagosomes in proliferation, their dramatic formation during the encystation of *E. invadens* strongly suggests that autophagy is involved in differentiation. The fact that the emergence of the Atg8-associated structures precedes morphological and biochemical changes (7, 10, 12, 47) during encystation strongly indicates that autophagy is a prerequisite for and plays an important role in encystation. It is also important to note that most of the differentially expressed genes previously identified (47) were up-regulated between 22 and 24 h after encystation induction, which coincides with the peak of autophagosome formation. The rapid degradation and recycling of cellular components via autophagy may be advantageous during encystation, which requires the dramatic and swift reorganization of cellular structures and organelles.

ACKNOWLEDGMENTS

We thank Asao Makioka, Jikei University, for providing the IP-1 strain and also technical help; Dan Sato for purification of the anti-EhAtg8 antibody; Yoko Yamada for production of the antibody; Eiryo Kawakami, University of Tokyo, for technical help; and all members of our laboratory for their technical assistance and discussions.

This work was supported in part by Grants-in-Aid for Scientific Research from the Ministry of Education, Culture, Sports, Science and Technology of Japan (17390124, 17790282, 18050006, 18073001); a grant for Research on Emerging and Reemerging Infectious Diseases from the Ministry of Health, Labor and Welfare (01712004); and a grant for the Project to Promote the Development of Anti-AIDS Pharmaceuticals from the Japan Health Sciences Foundation (KA11501) to T.N.

REFERENCES

1. **Ali, V., Y. Shigeta, U. Tokumoto, Y. Takahashi, and T. Nozaki.** 2004. An intestinal parasitic protist, Entamoeba histolytica, possesses a non-redundant nitrogen fixation-like system for iron-sulfur cluster assembly under anaerobic conditions. J. Biol. Chem. **279:**16863–16874.
2. **Amar, N., G. Lustig, Y. Ichimura, Y. Ohsumi, and Z. Elazar.** 2006. Two newly identified sites in the ubiquitin-like protein Atg8 are essential for autophagy. EMBO Rep. **7:**635–642.
3. **Andrade, R. M., M. Wessendarp, M. J. Gubbels, B. Striepen, and C. S. Subauste.** 2006. CD40 induces macrophage anti-*Toxoplasma gondii* activity by triggering autophagy-dependent fusion of pathogen-containing vacuoles and lysosomes. J. Clin. Investig. **116:**2366–2377.
4. **Besteiro, S., R. A. Williams, L. S. Morrison, G. H. Coombs, and J. C. Mottram.** 2006. Endosome sorting and autophagy are essential for differentiation and virulence of *Leishmania major*. J. Biol. Chem. **281:**11384–11396.
5. **Campos-Gongora, E., F. Ebert, U. Willhoeft, S. Said-Fernandez, and E. Tannich.** 2004. Characterization of chitin synthases from *Entamoeba*. Protist **155:**323–330.
6. **Clark, C. G., C. M. Alsmark, M. Hofer, Y. Saito-Nakano, V. Ali, S. Marion, C. Weber, C. Mukherjee, I. Bruchhaus, E. Tannich, M. Leippe, T. Sicheritz-Ponten, P. G. Foster, J. Samuelson, C. J. Noel, R. P. Hirt, T. M. Embley, C. A. Gilchrist, B. J. Mann, U. Singh, J. P. Acmers, S. Bhattacharya, A. Bhattacharya, A. Lohia, N. Guillen, M. Duchene, T. Nozaki, and N. Hall.** Structure and content of *Entamoeba histolytica* genome. Adv. Parasitol., in press.
7. **Coppi, A., and D. Eichinger.** 1999. Regulation of *Entamoeba invadens* encystation and gene expression with galactose and N-acetylglucosamine. Mol. Biochem. Parasitol. **102:**67–77.
8. **Diamond, L. S., C. F. T. Mattern, and I. L. Bartgis.** 1972. Viruses of *Entamoeba histolytica*. J. Virol. **9:**326–341.
9. **Doelling, J. H., J. M. Walker, E. M. Friedman, A. R. Thompson, and R. D. Vierstra.** 2002. The APG8/12-activating enzyme APG7 is required for proper nutrient recycling and senescence in *Arabidopsis thaliana*. J. Biol. Chem. **277:**33105–33114.
10. **Ehrenkaufer, G. M., R. Haque, J. A. Hackney, D. J. Eichinger, and U. Singh.** 2007. Identification of developmentally regulated genes in *Entamoeba histolytica*: insights into mechanisms of stage conversion in a protozoan parasite. Cell. Microbiol. **9:**1426–1444.
11. **Eichinger, D.** 2001. Encystation in parasitic protozoa. Curr. Opin. Microbiol. **4:**421–426.
12. **Gonzalez, J., G. Bai, U. Frevert, E. J. Corey, and D. Eichinger.** 1999. Proteasome-dependent cyst formation and stage-specific ubiquitin mRNA accumulation in *Entamoeba invadens*. Eur. J. Biochem. **264:**897–904.
13. **Gutierrez, M. G., S. S. Master, S. B. Singh, G. A. Taylor, M. I. Colombo, and V. Deretic.** 2004. Autophagy is a defense mechanism inhibiting BCG and *Mycobacterium tuberculosis* survival in infected macrophages. Cell **119:**753–766.
14. **Hamasaki, M., T. Noda, and Y. Ohsumi.** 2003. The early secretory pathway contributes to autophagy in yeast. Cell Struct. Funct. **28:**49–54.
15. **Huang, W. P., and D. J. Klionsky.** 2002. Autophagy in yeast: a review of the molecular machinery. Cell Struct. Funct. **27:**409–420.
16. **Ichimura, Y., Y. Imamura, K. Emoto, M. Umeda, T. Noda, and Y. Ohsumi.** 2004. In vivo and in vitro reconstitution of Atg8 conjugation essential for autophagy. J. Biol. Chem. **279:**40584–40592.
17. **Ichimura, Y., T. Kirisako, T. Takao, Y. Satomi, Y. Shimonishi, N. Ishihara, N. Mizushima, I. Tanida, E. Kominami, M. Ohsumi, T. Noda, and Y. Ohsumi.** 2000. A ubiquitin-like system mediates protein lipidation. Nature **408:**488–492.
18. **Ishihara, N., M. Hamasaki, S. Yokota, K. Suzuki, Y. Kamada, A. Kihara, T. Yoshimori, T. Noda, and Y. Ohsumi.** 2001. Autophagosome requires specific

early Sec proteins for its formation and NSF/SNARE for vacuolar fusion. Mol. Biol. Cell **12:**3690–3702.
19. **Kabeya, Y., N. Mizushima, T. Ueno, A. Yamamoto, T. Kirisako, T. Noda, E. Kominami, Y. Ohsumi, and T. Yoshimori.** 2000. LC3, a mammalian homologue of yeast Apg8p, is localized in autophagosome membranes after processing. EMBO J. **19:**5720–5728.
20. **Kirisako, T., Y. Ichimura, H. Okada, Y. Kabeya, N. Mizushima, T. Yoshimori, M. Ohsumi, T. Takao, T. Noda, and Y. Ohsumi.** 2000. The reversible modification regulates the membrane-binding state of Apg8/Aut7 essential for autophagy and the cytoplasm to vacuole targeting pathway. J. Cell Biol. **151:**263–276.
21. **Klionsky, D. J., J. M. Cregg, W. A. Dunn, Jr., S. D. Emr, Y. Sakai, I. V. Sandoval, A. Sibirny, S. Subramani, M. Thumm, M. Veenhuis, and Y. Ohsumi.** 2003. A unified nomenclature for yeast autophagy-related genes. Dev. Cell **5:**539–545.
22. **Kuma, A., N. Mizushima, N. Ishihara, and Y. Ohsumi.** 2002. Formation of the approximately 350-kDa Apg12-Apg5.Apg16 multimeric complex, mediated by Apg16 oligomerization, is essential for autophagy in yeast. J. Biol. Chem. **277:**18619–18625.
23. **Levine, B.** 2005. Eating oneself and uninvited guests: autophagy-related pathways in cellular defense. Cell **120:**159–162.
24. **Levine, B., and D. J. Klionsky.** 2004. Development by self-digestion: molecular mechanisms and biological functions of autophagy. Dev. Cell **6:**463–477.
25. **Levine, B., and J. Yuan.** 2005. Autophagy in cell death: an innocent convict? J. Clin. Investig. **115:**2679–2688.
26. **Liang, K., Y. Lin, Y. Zhang, Z. Chen, P. Zhang, and H. Zhang.** 2004. Developmental expression of amphioxus GABAA receptor-associated protein-like 2 gene. Dev. Genes Evol. **214:**339–341.
27. **Lindmo, K., and H. Stenmark.** 2006. Regulation of membrane traffic by phosphoinositide 3-kinases. J. Cell Sci. **119:**605–614.
28. **Ling, Y. M., M. H. Shaw, C. Ayala, I. Coppens, G. A. Taylor, D. J. Ferguson, and G. S. Yap.** 2006. Vacuolar and plasma membrane stripping and autophagic elimination of *Toxoplasma gondii* in primed effector macrophages. J. Exp. Med. **203:**2063–2071.
29. **Liu, Y., M. Schiff, K. Czymmek, Z. Talloczy, B. Levine, and S. P. Dinesh-Kumar.** 2005. Autophagy regulates programmed cell death during the plant innate immune response. Cell **121:**567–577.
30. **Lum, J. J., R. J. DeBerardinis, and C. B. Thompson.** 2005. Autophagy in metazoans: cell survival in the land of plenty. Nat. Rev. Mol. Cell Biol. **6:**439–448.
31. **Makioka, A., M. Kumagai, H. Ohtomo, S. Kobayashi, and T. Takeuchi.** 2001. Inhibition of encystation of *Entamoeba invadens* by wortmannin. Parasitol. Res. **87:**371–375.
32. **Makioka, A., M. Kumagai, H. Ohtomo, S. Kobayashi, and T. Takeuchi.** 2000. Effect of the antitubulin drug oryzalin in the encystation of *Entamoeba invadens*. Parasitol. Res. **86:**625–629.
33. **Martinez-Palomo, A., and M. Martinez-Baez.** 1983. Selective primary health care: strategies for control of disease in the developing world. X. Amebiasis. Rev. Infect. Dis. **5:**1093–1102.
34. **Melendez, A., Z. Talloczy, M. Seaman, E. L. Eskelinen, D. H. Hall, and B. Levine.** 2003. Autophagy genes are essential for dauer development and life-span extension in *C. elegans*. Science **301:**1387–1391.
35. **Mizushima, N., Y. Ohsumi, and T. Yoshimori.** 2002. Autophagosome formation in mammalian cells. Cell Struct. Funct. **27:**421–429.
36. **Nair, U., and D. J. Klionsky.** 2005. Molecular mechanisms and regulation of specific and nonspecific autophagy pathways in yeast. J. Biol. Chem. **280:**41785–41788.
37. **Nakagawa, I., A. Amano, N. Mizushima, A. Yamamoto, H. Yamaguchi, T. Kamimoto, A. Nara, J. Funao, M. Nakata, K. Tsuda, S. Hamada, and T. Yoshimori.** 2004. Autophagy defends cells against invading group A *Streptococcus*. Science **306:**1037–1040.
38. **Nimmerjahn, F., S. Milosevic, U. Behrends, E. M. Jaffee, D. M. Pardoll, G. W. Bornkamm, and J. Mautner.** 2003. Major histocompatibility complex class II-restricted presentation of a cytosolic antigen by autophagy. Eur. J. Immunol. **33:**1250–1259.
39. **Nozaki, T., T. Asai, S. Kobayashi, F. Ikegami, M. Noji, K. Saito, and T. Takeuchi.** 1998. Molecular cloning and characterization of the genes encoding two isoforms of cysteine synthase in the enteric protozoan parasite *Entamoeba histolytica*. Mol. Biochem. Parasitol. **97:**33–44.
40. **Nozaki, T., T. Asai, and T. Takeuchi.** 1997. Codon usage in *Entamoeba histolytica*, *E. dispar* and *E. invadens*. Parasitol. Int. **46:**105–109.
41. **Otto, G. P., M. Y. Wu, N. Kazgan, O. R. Anderson, and R. H. Kessin.** 2003. Macroautophagy is required for multicellular development of the social amoeba *Dictyostelium discoideum*. J. Biol. Chem. **278:**17636–17645.
42. **Petiot, A., E. Ogier-Denis, E. F. Blommaart, A. J. Meijer, and P. Codogno.** 2000. Distinct classes of phosphatidylinositol 3′-kinases are involved in signaling pathways that control macroautophagy in HT-29 cells. J. Biol. Chem. **275:**992–998.
43. **Pua, H. H., I. Dzhagalov, M. Chuck, N. Mizushima, and Y. W. He.** 2007. A critical role for the autophagy gene Atg5 in T cell survival and proliferation. J. Exp. Med. **204:**25–31.
44. **Qu, X., J. Yu, G. Bhagat, N. Furuya, H. Hibshoosh, A. Troxel, J. Rosen, E. L. Eskelinen, N. Mizushima, Y. Ohsumi, G. Cattoretti, and B. Levine.** 2003. Promotion of tumorigenesis by heterozygous disruption of the beclin 1 autophagy gene. J. Clin. Investig. **112:**1809–1820.
45. **Reggiori, F., T. Shintani, U. Nair, and D. J. Klionsky.** 2005. Atg9 cycles between mitochondria and the pre-autophagosomal structure in yeasts. Autophagy **1:**101–109.
46. **Sambrook, J., and D. W. Russell.** 2001. Molecular cloning: a laboratory manual, 3rd ed. Cold Spring Harbor Laboratory Press, Cold Spring Harbor, NY.
47. **Sanchez, L., V. Enea, and D. Eichinger.** 1994. Identification of a developmentally regulated transcript expressed during encystation of Entamoeba invadens. Mol. Biochem. Parasitol. **67:**125–135.
48. **Sarbassov, D. D., S. M. Ali, and D. M. Sabatini.** 2005. Growing roles for the mTOR pathway. Curr. Opin. Cell Biol. **17:**596–603.
49. **Schmid, D., J. Dengjel, O. Schoor, S. Stevanovic, and C. Munz.** 2006. Autophagy in innate and adaptive immunity against intracellular pathogens. J. Mol. Med. **84:**194–202.
50. **Shintani, T., W. P. Huang, P. E. Stromhaug, and D. J. Klionsky.** 2002. Mechanism of cargo selection in the cytoplasm to vacuole targeting pathway. Dev. Cell **3:**825–837.
51. **Strawbridge, A. B., and J. S. Blum.** 2007. Autophagy in MHC class II antigen processing. Curr. Opin. Immunol. **19:**87–92.
52. **Sugawara, K., N. N. Suzuki, Y. Fujioka, N. Mizushima, Y. Ohsumi, and F. Inagaki.** 2005. Structural basis for the specificity and catalysis of human Atg4B responsible for mammalian autophagy. J. Biol. Chem. **280:**40058–40065.
53. **Suzuki, K., Y. Kubota, T. Sekito, and Y. Ohsumi.** 2007. Hierarchy of Atg proteins in pre-autophagosomal structure organization. Genes Cells **12:**209–218.
54. **Tanida, I., T. Ueno, and E. Kominami.** 2004. LC3 conjugation system in mammalian autophagy. Int. J. Biochem. Cell Biol. **36:**2503–2518.
55. **Tsukada, M., and Y. Ohsumi.** 1993. Isolation and characterization of autophagy-defective mutants of *Saccharomyces cerevisiae*. FEBS Lett. **333:**169–174.
56. **Uritani, M., H. Hidaka, Y. Hotta, M. Ueno, T. Ushimaru, and T. Toda.** 2006. Fission yeast Tor2 links nitrogen signals to cell proliferation and acts downstream of the Rheb GTPase. Genes Cells **11:**1367–1379.
57. **Van Dellen, K. L., A. Chatterjee, D. M. Ratner, P. E. Magnelli, J. F. Cipollo, M. Steffen, P. W. Robbins, and J. Samuelson.** 2006. Unique posttranslational modifications of chitin-binding lectins of *Entamoeba invadens* cyst walls. Eukaryot. Cell **5:**836–848.
58. **Wang, C. W., and D. J. Klionsky.** 2003. The molecular mechanism of autophagy. Mol. Med. **9:**65–76.
59. Reference deleted.
60. **Williams, R. A., L. Tetley, J. C. Mottram, and G. H. Coombs.** 2006. Cysteine peptidases CPA and CPB are vital for autophagy and differentiation in *Leishmania mexicana*. Mol. Microbiol. **61:**655–674.
61. **World Health Organization/Pan American Health Organization.** 1997. Amoebiasis. Wkly. Epidemiol. Rec. **72:**97–99.
62. **Yoshimoto, K., H. Hanaoka, S. Sato, T. Kato, S. Tabata, T. Noda, and Y. Ohsumi.** 2004. Processing of ATG8s, ubiquitin-like proteins, and their deconjugation by ATG4s are essential for plant autophagy. Plant Cell **16:**2967–2983.
63. **Yue, Z., S. Jin, C. Yang, A. J. Levine, and N. Heintz.** 2003. Beclin 1, an autophagy gene essential for early embryonic development, is a haploinsufficient tumor suppressor. Proc. Natl. Acad. Sci. USA **100:**15077–15082.

Editor: W. A. Petri, Jr.

Genes and Immunity (2008), 1–10

www.nature.com/gene

ORIGINAL ARTICLE

Gender and genetic control of resistance to intestinal amebiasis in inbred mice

S Hamano[1], S Becker[2], A Asgharpour[2], YPR Ocasio[2], SE Stroup[2], M McDuffie[3] and E Houpt[2]
[1]Department of Parasitology, Faculty of Medical Sciences, Kyushu University, Fukuoka, Japan; [2]Division of Infectious Diseases and International Health, Department of Medicine, University of Virginia, Charlottesville, VA, USA and [3]Department of Microbiology, University of Virginia, Charlottesville, VA, USA

Resistance to the establishment of intestinal Entamoeba histolytica infection is dependent on the inbred mouse strain. In this work we used the inbred strains B6 (resistant), CBA (susceptible), B6CBAF, and a backcross of B6CBAF, to CBA to further examine the genetic basis of resistance. Mouse genotype was assessed with single nucleotide polymorphism and microsatellite markers and infection assessed by culture 9 days after intracecal E. histolytica challenge. The backcross population showed a male predisposition to culture positivity ($P<0.002$). F1 genotype at two loci on chromosomes 1 and 2 exhibited suggestive linkage with resistance to infection ($P=0.0007$ and 0.0200). Additional suggestive quantitative trait locus were observed on chromosomes 1, 9 and 13 for cecal parasite antigen load and histologic evidence of inflammation. Infection in C3H × B6 recombinant inbred mice supported the mapping data. Candidate B6 genes on chromosomes 1 and 2 were examined by microarray analysis of epithelial tissues from B6 vs CBA mice. This work shows a male predisposition to intestinal amebiasis and suggests that relatively few B6 loci can confer resistance in inbred mice. Future identification of regional candidate genes has implications for understanding the human variability to amebic infection.
Genes and Immunity advance online publication, 15 May 2008; doi:10.1038/gene.2008.37

Keywords: *parasite; protozoa; mucosa; Entamoeba; epithelium; infection*

Introduction

Entamoeba histolytica is the agent of amebic colitis and liver abscess and is responsible for a global mortality burden, second only to malaria, among parasitic diseases.[1] However not all infections result in disease. Bangladeshi children with similar exposure risk exhibit significant variability in susceptibility to both colonization and invasive infection.[2,3] Other reports confirm a colonization rate of up to 8% in endemic areas, yet only approximately 9% of colonized individuals develop symptoms.[4–6] For unknown reasons male gender appears to predispose toward progression to invasive disease, both colitis and liver abscess, but has a neutral effect on colonization rates.[7] Mechanisms of human resistance to the parasite have largely been studied at the adaptive immune level and show associations between fecal immunoglobin A and parasite-specific interferon gamma production with resistance to subsequent diarrheal episodes.[2,8,9] Comparatively little is known about mechanisms that protect against primary infection in the gut.

We have used a mouse model of intestinal amebiasis that is informative of this initial infection event. Intracecal inoculation of trophozoites[8,10,11] leads to patent infection and inflammation in certain strains of mice such as CBA or C3H (either TLR4 mutant or wild-type) while several other inbred mouse strains including B6 are highly resistant to infection, clearing trophozoites within hours. This timing suggests that B6 resistance is innate, or perhaps more appropriately termed 'natural,' because it occurs with relatively little histologic change and does not require an intact inflammatory response (for example, it is seen in severe combined immunodeficiency disease (SCID), IL-12p40 deficient, inducible nitric oxide synthase deficient, phagocyte oxidase deficient, MyD88 deficient or neutrophil-depleted B6 mice).[10,11] Bone marrow chimera experiments have shown that the resistance vs susceptibility of B6 vs CBA mice to this infection track with the strain's nonhematopoietic cells,[12] suggesting the host's epithelium governs this phenotype. Overall we conceptualize B6 mice as endowed with an inherently resistant epithelial response to the parasite, while that of the CBA is permissive to infection. One hypothesis is that B6 mucosa is deficient in binding to the parasite or its adhesin. Another hypothesis is that B6 epithelial cells undergo a phenotypically distinct and protective program upon interaction with the parasite. In this work we could not readily observe a defect in parasite adherence to the B6 mucus layer and therefore pursued potential B6 resistance genes through comparison of B6, CBA,

Correspondence: Dr E Houpt, Division of Infectious Diseases and International Health, Department of Medicine, University of Virginia, 409 Lane Rd., MR4 2144, PO Box 801363, Charlottesville, VA 22908-0136, USA.
E-mail: erh6k@virginia.edu
Received 10 January 2008; revised 31 March 2008; accepted 1 April 2008

B6CBAF$_1$ and N$_2$ backcross mice. To our surprise this work incidentally identified an effect of gender on primary susceptibility.

Results

B6 resistance is not associated with diminished parasite adherence to mucus layer

E. histolytica trophozoites initiate infection by adhering to colonic mucus through the parasite's galactose/*N*-acetyl-D-galactosamine inhibitable (Gal/GalNAc) lectin.[13,14] We therefore sought to examine the hypothesis that B6 resistance was contributed by dysfunctional parasite adherence to cecal mucus. First we examined binding of purified *E. histolytica* Gal/GalNac lectin to cecal mucus and epithelium between strains but there were no apparent differences by histochemistry (Figure 1a). Next we preincubated intestinal washes from CBA and B6 mice with the ameba but found no alteration in strain susceptibility upon subsequent challenge (culture positivity rates 9 days post-challenge 1/17, 1/16, 11/30 and 11/27 for B6 mice injected with ameba incubated with B6 washes, B6 mice/CBA washes, CBA mice/B6 washes and CBA mice/CBA washes; $P<0.03$ for mouse strain, $P=$NS for intestinal washes). Finally we examined susceptibility of B6 mice deficient in Muc2, the most abundant secreted mucin in the colon[15] and known to prevent *E. histolytica* adherence *in vitro*.[16] For such experiments on the resistant B6 background we killed the mice at 3 days post-challenge to look for evidence of ameba histologically, however the Muc2KO mice remained resistant to wild-type levels, with ameba or inflammation rarely seen (Figures 1b and c).

B6CABF$_1$ × CBA backcross N$_2$ mice exhibit intermediate susceptibility to amebiasis and show a male predisposition to infection

As we could not demonstrate any obvious role for differential adherence to intestinal mucus between strains, we undertook a less biased forward approach to identify genetic loci associated with B6 resistance to primary infection. First we examined susceptibility in F1 mice and found that B6CBAF$_1$ mice (offspring of a B6 female × CBA male cross) or the reciprocal CBAB6F$_1$ mice were resistant (infection rate = 2/28 and 0/6, respectively, based on culture 1 week after challenge, with no difference between males or females) indicating that resistance was dominant and susceptibility recessive.

In order to map B6 loci that confer resistance, we generated N$_2$ mice using a cross between B6CBAF$_1$ female and CBA male mice. To efficiently examine the genetics of susceptibility with the fewest numbers of mice, all cohorts shown in the experiments of Figure 2 were pretreated with dexamethasone because this maneuver raises the susceptibility of CBA mice (from ~60 to ~95%) but has little effect on B611 or F1 mice (for example, B6CBAF$_1$ infection rate = 5/23 and CBAB6F$_1$ infection rate = 2/24 with dexamethasone, compared to

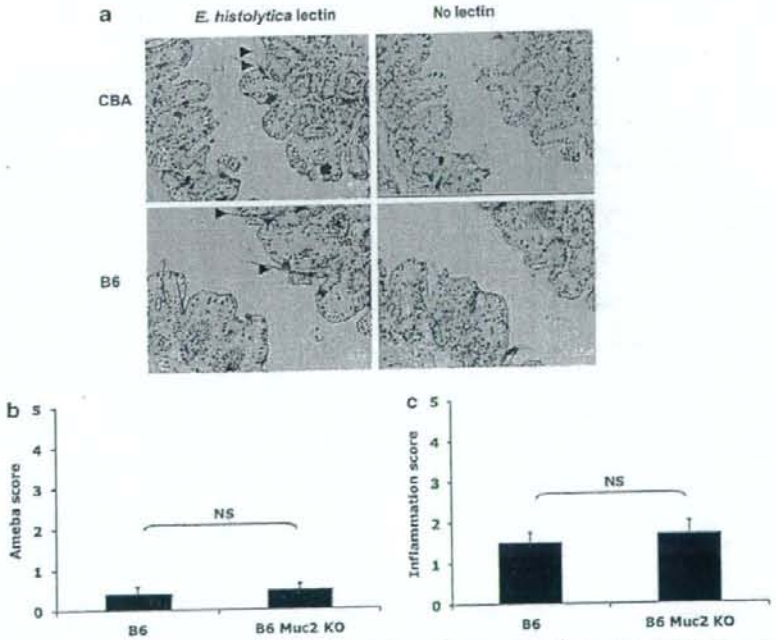

Figure 1 B6 resistance is not associated with diminished mucus binding. (a) Binding of purified *Entamoeba histolytica* Gal/GalNac adherence lectin to cecal epithelium was compared between naive B6 and CBA cecal tissue by histochemistry. (b) Histologic ameba score and (c) inflammation score was evaluated in B6 and Muc2KO mice 3 days after intracecal challenge with ameba. $n=18$ B6 Muc2KO vs 17 B6 WT littermates, respectively; $P=$NS.

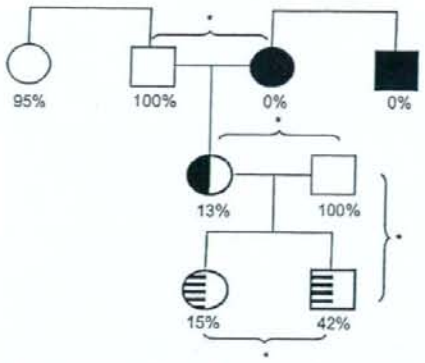

Figure 2 Susceptibility of CBA, B6, F1 and N2 mice. CBA (open symbols) and B6 (closed symbols) mice were bred as indicated and challenged intracecally with *Entamoeba histolytica* trophozoites at 6–10 weeks of age. Susceptibility to establishment of infection was determined by cecal culture upon killing 7–10 days post-challenge. Percentages of infected mice are shown at each generation, $n = 20, 8, 12, 12, 16, 55$ and 62 for female CBA, male CBA, female B6, male B6, female F_1, female N_2 and male N_2 mice, respectively. $^*P<0.05$ for infection rate. Proportions of open vs closed shading represent contribution of CBA vs B6 genetic material; circles = female, squares = male. Data represent several experiments in mice treated with 0.2 mg dexamethasone on days −3, −2, −1 and 0 to ensure maximal phenotypic separation between CBA and B6 mice.

B6CBAF$_1$ infection rate = 2/28 and CBAB6F$_1$ infection rate = 0/6, P = NS; no difference between males or females, data not shown). N_2 mice (117) were intracecally challenged with *E. histolytica* trophozoites and killed after 9 days. Of these 117 N_2 mice, 36 exhibited patent *E. histolytica* infection by cecal culture (infection rate, 31%). We detected a significant difference in infection rate between males and females in this N_2 population (27/62 male mice infected vs 9/55 female mice; $P = 0.002$). Additionally, infected male mice had a higher parasite burden than infected females according to enzyme-linked immunosorbent assay (ELISA; 0.54 ± 0.11 vs 0.16 ± 0.11, $P = 0.04$; $n = 27$ and 9). Thus far we have not documented a male effect on infection rate in the pure CBA, B6 or F1 strains, perhaps due to sample size issues, however we have observed a significant male predisposition in the FVB strain (for example, 15/18 FVB males infected vs 10/25 females based on culture 5 days post-challenge with no dexamethasone pretreatment; $P < 0.05$).

This infection rate of 42% in male N_2 mice suggested that relatively few co-inherited B6 alleles could impart resistance (for example, 1 or 2 genes should impart ~25 or ~50% infection rate, respectively, given 0% infection rate in B6 male and 100% in CBA male). Likewise, the low infection rate of 15% in female N_2 suggested that several CBA genes must be inherited for susceptibility in females.

Loci on chromosomes 1 and 2 correlate with resistance to intestinal amebiasis

In order to examine candidate B6 genes that could impart resistance in the N_2 population, we fixed the CBA Y chromosome and compared the 27 infected vs 25 uninfected N_2 males by whole-genome scan (Table 1).

Table 1 Microsatellite and SNP markers used for whole-genome scan

Chromosome	*Markers*	*Chromosome position (approximate bp)*
1	rs3658242	4 147 733
	rs3024171	6 479 671
	rs3706453	10 022 182
	rs3684370	16 188 620
	rs13475752	19 945 224
	rs3725641	29 062 181
	rs3695988	30 064 384
	rs3707642	32 883 065
	rs4136282	43 879 038
	rs3720019	59 025 545
	rs3697376	65 048 023
	rs3022803	68 518 728
	rs4222476	79 140 199
	rs3677697	80 071 474
	rs3022828	93 044 874
	rs3680832	118 653 878
	D1Mit217	122 498 355
	rs3710036	149 729 600
	rs3710904	187 152 679
	D1Mit155	196 255 163
2	rs3695983	6 153 138
	rs3689602	30 268 356
	rs13476468	44 473 712
	rs3022884	54 417 652
	rs3690911	56 262 283
	rs13476522	(not mapped)
	rs4223211	69 634 901
	rs3699089	75 946 661
	rs3668963	79 192 487
	rs4223268	93 260 019
	rs3686727	99 962 752
	rs3656441	103 087 510
	rs3022892	109 840 163
	rs4223406	113 667 509
	rs3691456	118 811 005
	rs3674772	122 897 952
	rs3662211	129 970 691
	rs3726475	138 397 679
	rs3690107	145 704 738
	rs4223557	150 107 206
	rs4223564	154 704 249
	rs3022939	161 846 330
	rs3680965	180 173 682
3	rs3680834	11 364 825
	rs3659585	32 420 597
	rs4223979	60 881 246
	rs4224040	88 405 297
	rs3708141	117 412 146
	rs3654999	153 537 571
4	rs3694594	3 163 293
	rs3706812	33 090 337
	rs3654495	59 137 998
	rs4136370	88 963 090
	rs3673616	123 641 393
	rs3680364	152 370 035
5	D5Mit346	4 879 428
	rs13478101	6 996 931
	D5Mit255	55 345 578
	rs3690045	88 600 282
	rs3023056	123 036 374
6	rs3661828	3 165 742
	D6Mit86	4 414 884
	rs3699842	32 777 082
	rs3708822	89 830 709
	rs3727110	122 832 668
	D6Mit15	146 377 508
	D6Mit201	146 582 003
7	rs3710949	33 124 503
	D7Mit340	4 578 848
	rs3024018	62 470 203

Table 1 Continued

Chromosome	*Markers*	*Chromosome position (approximate bp)*
	rs3705245	89 854 074
	D7Mit222	120 077 980
	rs3690034	126 850 930
	D7Mit12	143 722 527
8	rs3675426	30 815 477
	D8Mit191	36 243 839
	rs3089230	67 095 184
	rs3089148	92 310 176
	D8Mit242	104 283 476
	rs6296597	122 145 801
9	rs3023961	3 974 986
	D9Mit330	46 949 949
	rs4227706	62 567 226
	rs3696932	92 110 048
	rs3679771	112 768 715
10	rs3663844	6 356 294
	D10Mit123	9 952 319
	rs13480578	34 297 659
	rs13480619	57 472 268
	rs3713441	90 418 025
	D10Mit12	98 936 190
	rs4136978	126 605 953
11	rs3659787	4 383 867
	D11Mit152	24 126 273
	rs3696538	39 186 264
	rs3023311	59 601 495
	D11Mit4	68 422 759
	rs3682081	90 284 270
	D11Mit124	99 051 969
12	rs3675632	3 567 742
	rs3711295	26 348 059
	rs3677704	61 096 491
	D12Mit201	73 392 448
	rs3719660	92 258 360
	rs3686631	112 485 205
13	rs3701757	15 605 056
	rs3679151	41 944 861
	D13Mit13	56 582 797
	rs3675592	90 070 327
	rs3724755	112 195 257
	D13Mit35	120 128 451
14	rs3689508	5 057 217
	rs3719262	23 692 210
	D14Mit60	47 717 468
	rs3664667	57 409 125
	rs3712154	102 919 945
15	rs3715343	6 003 109
	rs3720676	32 992 272
	rs3702158	57 312 070
	D15Mit63	65 076 746
	rs3023429	102 265 828
	D15Mit35	103 347 764
16	rs4153115	5 057 146
	D16Mit60	32 704 177
	rs4174474	37 982 634
	D16Mit158	80 530 693
	rs4231259	72 308 813
	rs4221067	96 012 232
17	rs3660203	6 958 021
	D17Mit113	12 172 308
	D17Mit16	33 737 692
	D17Mit13	35 216 590
	D17Mit10	(not mapped)
	rs3023456	65 900 970
	D17Mit39	74 681 434
	rs4231722	85 479 538
18	rs4231742	11 079 095
	rs3707236	22 167 340
	rs3023468	63 864 232
	rs3670234	86 838 611
19	rs3023688	7 236 613
	rs13483595	32 472 038
	rs3023517	59 767 603
X	rs13476522	(not mapped)
	rs3684845	38 424 585
	rs3161045	55 628 339
	rs3709255	84 188 766
	rs3702256	116 747 330
	DXMit149	124 541 535
	rs3698078	146 295 362

We carried out c2 test because infection rate is categorical data (culture positive Y/N) and found that an F_1 genotype at proximal chromosome 1 (rs3725641/29 062 181 bp, $c2 = 10.23$, $P = 0.0007$) and middle chromosome 2 (rs3690911/56 262 283 bp, $c2 = 4.22$, $P = 0.0200$) exhibited suggestive linkage with resistance to infection (Figure 3a). Paradoxically, mice homozygous for CBA at proximal chromosome 17 were also resistant (rs3660203/6 958 021 bp and D17Mit113/12 172 308 bp, $c2 = 3.88$, $P = 0.0244$). Upon increasing the resolution of genome scan via 20 additional genetic markers across the chromosomes 1 and 2 intervals we observed that the chromosome 1 interval continued to show evidence suggestive of linkage from the telomere until rs3022803/68 518 728 bp, $c2 = 6.52$, $P = 0.0053$), with strongest loci at positions rs3684370/16 188 620 bp ($c2 = 10.39$, $P = 0.0006$) and rs3695988/30 064 384 bp ($c2 = 10.39$, $P = 0.0006$; Figure 3b). Likewise, suggestive linkage existed for most of the chromosome 2 region between rs3022884/54 417 652 bp and rs3662211/129 970 691 bp ($c2 = 5.26$, $P = 0.0109$ and $c2 = 7.00$, $P = 0.0041$, respectively; Figure 3b). Additionally, suggestive linkage persisted for both chromosomes 1 and 2 loci when all 117 mice including females were added to the analysis: proximal chromosome 1 rs3684370/16 188 620 bp ($c2 = 8.83$, $P = 0.001$) and middle chromosome 2 rs3022884/54 417 652 bp ($c2 = 6.48$, $P = 0.005$).

The effects of the chromosomes 1 and 2 alleles appeared to be additive. In particular, only 17% of the N_2 mice homozygous for CBA alleles at both loci were resistant (Figure 3c). N_2 mice of F1 genotype at either chromosome 1 (rs3684370/16 188 620) or chromosome 2 (rs3662211/129 970 691 bp) loci exhibited intermediate levels of resistance (46 and 36%, respectively) while N_2 mice of F1 genotype at both loci were highly resistant (94%; $P \leqslant 0.01$ vs other groups).

Genetic determinants for levels of ameba antigen and inflammation scores

While susceptibility to the establishment of infection (culture positive Y/N) is the simplest and most fundamental phenotype of this model we also performed quantitative trait locus (QTL) analysis of N_2 mice for the continuous variables of cecal amebic antigen and histologic inflammation score. Based on significance thresholds determined by permutation analysis (5000 replicates), our genome-wide scan of N_2 mice revealed suggestive QTLs for cecal antigen within the chromosome 1 region (rs3024171/6 479 671 bp and rs3684370/16 188 620 bp,

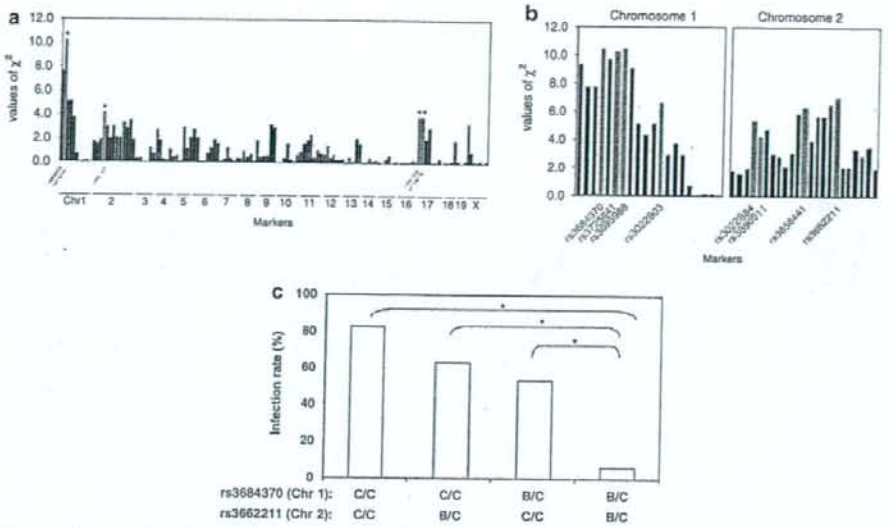

Figure 3 Resistance to intestinal amebiasis in N_2 mice is linked to F_1 B6/CBA loci on chromosomes 1 and 2. N_2 mice (117) were intracecally challenged with *Entamoeba histolytica* trophozoites at 6–10 weeks of age. (a) Infected male vs uninfected males were examined by whole genome analysis to identify F_1 B6/CBA loci that correlated with resistance. Asterisks indicate the peak of χ^2-score at each locus. (b) Extents of suggestive chromosome 1 and 2 loci were determined through an additional 20 genetic markers. (c) Infection rate is shown stratified per chromosomes 1 and 2 loci in N_2 mice ($n=12$, 11, 13, 16; $^*P<0.01$).

likelihood ratio statistic (LRS) = 7.3, $P=0.0068$, where LRS > 6.8 is suggestive of linkage and LRS > 12.6 is significant) as well as a new locus on proximal chromosome 13 (rs3679151/41 944 861 bp, LRS = 7.3, $P=0.0071$). In contrast, the same analysis based on histologic inflammation score yielded a suggestive QTL on chromosome 9 (rs3679771/112 768 715 bp, LRS = 8.8, $P=0.0030$ where LRS > 7.3 is suggestive and LRS > 13.6 is significant). These data suggest that genetic mechanisms controlling establishment of infection by the parasite (that is, infection rate, loci on chromosomes 1 and 2) may be distinct from those that control parasite burden during later infection (that is, cecal ELISA, chromosomes 1 and 13) and the resultant inflammatory response (that is, inflammation score, chromosome 9).

Combined gene effects

We next examined whether two or more loci could yield combined effects. Using permutation analysis we observed two combined effects that were again of suggestive significance for infection rate: rs3662211/Chr1-129 970 691 plus rs3024018/Chr7-62 470 203 (LRS 24.4 where > 20.6 is 'suggestive') and rs3654495/Chr4-59 137 998 plus rs3024018/Chr7-62 470 203 (LRS 21.1). Likewise, there were three combined effects that were of suggestive significance for cecal antigen: rs3022884/Chr2-54 417 652 plus rs4231722/Chr17-85 479 538 (LRS 26.1 where > 22.2 is 'suggestive'), rs3725641/Chr1-29 062 181 plus rs3022803/Chr1-68 518 728 (LRS 25.8) and rs13476468/Chr2-44 473 712 plus rs4231722/Chr17-85 479 538 (LRS 23.4). Finally, there were two combined effects that were of suggestive significance for inflammation score: rs3706812/Chr 4-33 090 337 plus rs3024018/Chr7-62 470 203 (LRS 22.5 where > 21.0 is 'suggestive') and rs3654495/Chr4-59 137 998 plus rs3024018/Chr7-62 470 203 (LRS 21.3). This suggests that additional loci on chromosomes 4, 7 and 17 may interact with those of chromosomes 1 or 2 to impact the establishment of infection, parasite burden or inflammation.

Effect of B6 alleles on chromosomes 1 and 2 loci on amebic infection in vivo

We next sought to validate our mapping results on chromosomes 1 and 2 using genotypically defined mice. Although no defined recombinant inbred or consomic panels are available for the CBA/B6 strain combination, we were able to obtain recombinant inbred mice derived from progenitor strains C3H/HeJ and B6 (BXH). The C3H and CBA strains are both susceptible in our model and are genetically similar, derived from the same 1920 cross between a Bagg albino female and a DBA male.[17] The BXH14/TyJ mouse is homozygous for C3H/HeJ alleles throughout the entire identified chromosome 1 and most of the chromosome 2 loci. For these studies no dexamethasone was administered which could confound effects on host genes. Given the known high-level resistance of B6 mice, these experiments were shortened to 24 h post-challenge and numbers of ameba was assessed by histology, a more discriminatory measure than culture or antigen at such an early time point.[12] Ameba score indicated that BXH14/TyJ mice were similarly susceptible to infection as C3H mice by this measure (P = NS vs C3H, $P=0.01$ vs B6; Figure 4), compatible with the notion that the chromosomes 1 and 2 loci are relevant.

Candidate genes at chromosomes 1 and 2 loci

Based on our previous findings that infection in this model is limited to the cecum and that mouse strain resistance tracks with nonhematopoietic cells,[12] a

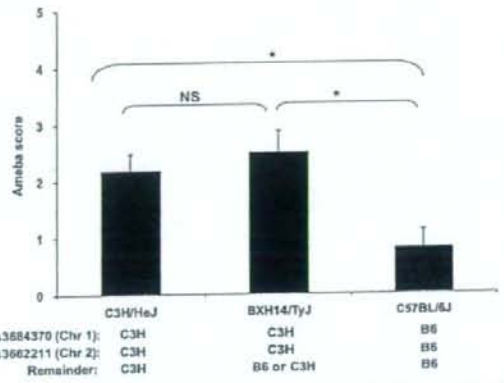

Figure 4 Correlation of resistance in B6 mice with chromosomes 1 and 2 loci. C3H/HeJ, BXH14/TyJ and B6 mice were challenged with *Entamoeba histolytica* trophozoites and killed at 24 h for evaluation of infection by histologic ameba score ($n = 11$, 8, 10, respectively; $^*P < 0.05$).

possible hypothesis is that genetic control of resistance resides at the level of the cecal epithelium. As genetic differences between CBA and B6 may be observable at the level of transcription we examined mRNA expression by microarray in stripped cecal epithelial tissues from naive CBA and B6 mice. Of 45 037 genes or expressed sequence tags probed with the Affymetrix MOE430 2.0 arrays, 954 were found to be differentially regulated in these two strains using a conventional D-chip analysis. Among genes with dysregulated expression more than 1.75-fold, 28 candidates localized to the relevant regions on chromosomes 1 or 2 (shown in Table 2). The expression of several upregulated B6 'resistance' candidate genes *Ctdspl2*, *Trp53bp1* and *Spata5l1* and upregulated CBA 'susceptibility' candidate genes *Tmtm87a* and *Pldn* showed consonant results by reverse transcriptase (RT)–PCR, per the validation methodology of Miron *et al*.[18] (Supplementary Figure 1, correlation coefficient = 0.80, $P = 0.028$). Full access to the microarray data including candidate genes at chromosomes 4, 7, 9, 13, and 17 can be found at https://genes.med.virginia.edu/public_data/index.cgi under 'Eric_Houpt_CBAvsB6naive'.

Discussion

The first clear finding from this work is that male gender can predispose toward intestinal amebiasis in mice, linking this mouse model strongly to human disease where male predominance has been repeatedly noted. The second finding from the backcross studies is that murine resistance to infection with *E. histolytica* may be imparted by relatively few genetic loci. Third, suggestive loci that associate with the initial infection rate were distinct from those of parasite burden and inflammation severity, suggesting that these phenomena may be under distinct host control.

Demonstration of a male predisposition to amebiasis was clearly dependent on the strength of the genetic susceptibility, with its effects only clearly seen in animals with inheritance of some resistance alleles. In the N_2 mouse population, male sex was associated with increases in both infection rate (culture positivity) and parasite burden once infected. A male increase in infection rate was also observed with the inbred FVB strain, but has not been seen in the strongly susceptible C3H or CBA or the resistant B6, presumably because sex chromosome-independent effects predominate in these strains. Although likely simplistic, we presently conceptualize the infection rate (culture positivity) as informing the event of colonization, while parasite burden and inflammation scores are measures of the severity of invasive disease. If this model is accurate, the latter finding of increased parasite burden in male mice is particularly supportive of the long-appreciated clinical finding that men are more predisposed to severe invasive amebiasis than women. The male predisposition to invasive amebiasis is striking and worldwide, with a male:female ratio of up to 7:1 for both colitis and liver abscess in several studies.[7] Mechanisms are unclear, however a male predominance has also been observed in a B6 mouse model of amebic liver abscess where it can be traced to a diminished innate interferon-γ response.[19] In other intestinal infection models such as *Campylobacter*, *Helicobacter* and *Strongyloides*,[20–24] a male predominance has also been observed and has been attributed broadly to testosterone effects.

Another important finding from this work was the suggestive association between B6 alleles on chromosomes 1 and 2 and resistance to parasite establishment in the gut. It is unclear whether such B6 loci actively confer resistance or whether CBA loci actively support the colonization of ameba in the gut, and that this permissiveness is then lost by default by replacement with B6 loci. One could argue the latter, that susceptibility is the abnormal phenotype and resistance is default, given previous work that shows the relative lack of an active histologic inflammatory response in B6 mice and their persistent resistance despite maneuvers to ablate inflammation.[10,11] As such, one would be interested in the pathologic role of upregulated epithelial CBA transcripts at the chromosomes 1 and 2 loci such as *Tmem87a* or *Pldn*, which unfortunately are presently undescribed (Table 2).

Alternatively one could argue that the presence of particular B6 genes could still actively confer resistance (for example, with minimal induction of inflammation) such as through control of production of an antimicrobial peptide. This would drive interest in the potential resistance functions of the upregulated B6 genes known to be involved in epithelial immunity (Table 2). Certainly lymphocyte antigen 96 (*Ly96*; MD-2) is an interesting candidate given its role in upregulating signaling through TLR4,[25] to which *E. histolytica* is known to bind.[18] However B6 resistance has not required MyD88,[11] therefore this candidate loses some enthusiasm, or one would need to invoke TRIF/MyD88-independent mechanisms of TLR4 activation.[26]

Transformation related p53 binding protein 1 was the most upregulated annotated B6 gene in the epithelium vs CBA (501-fold by microarray) and has been shown in other models of gut injury to function in maintaining DNA stability,[27] thus a possible role for this molecule in intestinal amebiasis could be envisioned. Other B6 transcripts of potential interest include apoptosis-related genes such as the proapoptotic gene *BCL2-like 11*. Epithelial apoptosis could be predicted to be either

Table 2 Chromosomes 1 and 2 resistance gene candidates

Gene	*Description*	*B6 (mean signal intensity, relative units)*	*CBA (mean signal intensity, relative units)*	*Fold change (CBA/B6)*	*Location*	*Affymetrix probe set*	P
C57BL/6J upregulated resistance candidates							
Ctdspl2[a]	(Sequences not annotated)	128.93	0.17	−755.56	2 E5|2 69.0 cM	1442424_at	0.019
Trp53bp1[a]	Transformation related protein 53 binding protein 1	141.63	0.28	−501.74	2 E5	1442316_x_at	0.019
Spata5l1[a]	Spermatogenesis associated 5-like 1	130.76	8.79	−14.87	2 E5	1455863_at	0.0023
LOC620009 /// Pdhb	Pyruvate dehydrogenase (lipoamide) beta	227.26	23.3	−9.75	1 A1/14 A1	1448214_at	0.00085
Arfgef1	(Sequences not annotated)	170.69	41.26	−4.14	1 A2	1444175_at	0.0045
Ckap2l	RIKEN cDNA 2610318C08 gene	464.55	117.19	−3.96	2 F1	1435938_at	0.023
Hisppd2a	RIKEN cDNA B430315C20 gene	220.15	69.93	−3.15	2 E5	1442466_a_at	0.000394
Tmem127	RIKEN cDNA 2310003P10 gene	951.3	381.05	−2.5	2 F1|2 62.4 cM	1433895_at	0.0085
Pdrg1	RIKEN cDNA 1110004D19 gene	534.52	225.67	−2.37	2 H1	1419933_at	0.014
Ly96[a]	Lymphocyte antigen 96	266.78	121.91	−2.19	1 A3	1449874_at	0.0024
Bcl2l11[a]	BCL2-like 11 (apoptosis facilitator)	820.09	377.97	−2.17	2 F3-G1	1456005_a_at	0.049
Cspp1	RIKEN cDNA 4930413O22 gene	363.26	178.12	−2.04	1 A2	1431405_a_at	0.025
Spred1	Sprouty protein with EVH-1 domain 1, related sequence	258.97	139.93	−1.85	2 E5	1423162_s_at	0.000999
Zfp106	Zinc finger protein 106	633.56	348.89	−1.82	2 F1|2 67.2 cM	1425331_at	0.0048
Rin2	15 days embryo head cDNA, RIKEN full-length enriched library, clone:D930006C05 product:unknown EST, full insert sequence	318.72	183.74	−1.73	2 G1	1441209_at	0.000507
Cds2	CDP-diacylglycerol synthase (phosphatidate cytidylyltransferase) 2	1834.58	1070.35	−1.71	2 F2|2 73.0 cM	1438957_x_at	0.027
1200015F23Rik	RIKEN cDNA 1200015F23 gene	1043.3	613.11	−1.7	2 E5	1428196_a_at	0.045
Sord	sorbitol dehydrogenase 1	860.62	546.68	−1.57	2 E5|2 66.0 cM	1426584_a_at	0.015
Epb4.1l1	Erythrocyte protein band 4.1-like 1	277.83	177.64	−1.56	2 H1|2 88.0 cM	1434575_at	0.024
Smox	Spermine oxidase	378.4	248.34	−1.52	2 F1	1424268_at	0.012
CBA/J upregulated susceptibility candidates							
Tmem87a[a]	RIKEN cDNA A930025J12 gene	88.19	975.22	11.06	2 E5	1424454_at	0.0014
Pldn[a]	(Sequences not annotated)	57.07	424.56	7.44	2 E5|2 67.6 cM	1457088_at	0.00027
Actc1	actin, alpha, cardiac	699.32	2084.01	2.98	2 E4|2 64.0 cM	1415927_at	0.0087
Eid1	CREBBP/EP300 inhibitory protein 1	522.35	1451.48	2.78	2 F1	1448406_at	0.019
Adal	RIKEN cDNA 4930578F03 gene	122.78	309.83	2.52	2 F1	1428198_at	0.018
BC052040	10 days neonate cerebellum cDNA, RIKEN full-length enriched library, clone:B930089B11 product:unknown EST, full insert sequence	79.86	182.11	2.28	2 E4	1460144_at	0.0011
Myl9	Myosin, light polypeptide 9, regulatory	2767.14	5264.28	1.9	2 H1	1452670_at	0.0089
Rbm39	Expressed sequence C79248	1448.29	2726.52	1.88	2 H1	1446147_at	0.020

[a]Gene dysregulation validated by qRT-PCR (Supplementary Figure 1).

protective or deleterious during amebiasis. In a SCID mouse model of amebic liver abscess, hepatocyte apoptosis plays a pathologic role in abscess formation.[28] In contrast in intestinal helminth models epithelial apoptosis is thought to be protective by maintaining crypt length and epithelial homeostasis.[29]

Beyond these chromosomes 1 and 2 loci that associate with resistance to the establishment of infection, the presence of other loci that associate with parasite burden once infected (chromosome 13) and the resultant inflammatory response (chromosome 9) suggest the presence of multiple layers of host control in amebiasis. The LRS scores for these loci were modest and should not be overinterpreted in the absence of confirmatory evidence in congenic or recombinant inbred strains. However the concept of sequential nodes of host control is in keeping with our working understanding of this model, which holds that amebic infection proceeds through multiple phases, step one being parasite survival amid the epithelium and step two being survival amid the inflammatory response. Therefore the possibility of distinct genetic loci that associate with these two steps was anticipated. As the mouse genome becomes annotated and whole genome association studies unfold from human amebiasis sites[9] it is hoped that findings such as these can be directly tested to shed light on the pathogenesis of this disease.

Materials and methods

Mice

C57BL/6, CBA/J, B6CBAF$_1$ (B6 × CBA) and BXH14/TyJ mice were purchased from The Jackson Laboratory (Bar Harbor, ME, USA). FVB mice were obtained from Craig Coopersmith (Washington University, St Louis, MO, USA). Muc2 KO mice were obtained from Anna Velcich (Albert Einstein Cancer Center/Montefiore Medical Center, New York, NY, USA) and tested against wild-type littermates. N_2 mice were bred by backcrossing B6CBAF$_1$ female with CBA/J male mice. Animals were maintained under specific pathogen-free conditions at the University of Virginia and were challenged at 4–8 weeks of age. The Institutional Animal Care and Use Committee approved all protocols. Recombinant inbred strain BXH14/TyJ contains unique, approximately equal proportions of genetic contributions from two progenitor C3H/HeJ and C57BL/6J inbred strains and is, importantly, homozygous for C3H/HeJ at whole chromosome 1 and the latter half of chromosome 2 (http://www.well.ox.ac.uk/mouse/INBREDS/RIL/BXH.shtml).

Parasites and intracecal inoculation

Trophozoites for intracecal injections were originally derived from laboratory strain HM1:IMSS (American Type Culture Collection, Manassas, VA, USA) that have been sequentially passaged *in vivo* through the mouse cecum. Cecal contents were cultured in trypsin-yeast-iron (TYI-S-33) medium supplemented with 25 U ml^{-1} penicillin and 25 mg ml^{-1} streptomycin. For all intracecal inoculations, trophozoites were grown to the log phase, counted with a hemacytometer and 2×10^6 trophozoites in 150 µl were injected thrice intracecally after laparotomy as described.[10] For select experiments dexamethasone was administered to mice 0.2 mg i.p. on days −3, −2, −1 and 0 to enhance susceptibility of CBA mice. For cecal wash experiments, cecal mucinous intestinal washes were prepared by flushing cecal contents with completed TYI media and centrifuging at 14 000 *g* × 10 min (simplified from Carlstedt *et al.*[30]). Supernatant was incubated 1:1 with an *E. histolytica* pellet of 2×10^6 trophozoites at 37 °C for 1 h and ameba were then injected intracecally.

Pathology and scoring of amebic colitis

Mice were killed and each cecum longitudinally bisected. One half of the cecum was placed in Hollande's fixative, cut into 3–5 equal cross sections, paraffin embedded and 4 mm sections were stained with hematoxylin and eosin. Histopathology was scored in blinded fashion for inflammation score and ameba score for each mouse as described previously.[16] To determine infection rate by culture, the contents of the other half of the cecum were rinsed in 1 ml phosphate-buffered saline (PBS) and cultured in TYI-S-33 medium. To determine infection severity 200 µl of this material was tested for *E. histolytica* antigen by ELISA (*E. histolytica* II test, Techlab, Blacksburg, VA, USA). ELISA values were normalized for background and positive control optic density.

Lectin histochemistry

Purified *E. histolytica* Gal/GalNAc lectin was prepared as previously described.[14] Frozen acetone-fixed sections of cecal tissue were stained with or without 20 µg lectin per ml × 30 min at room temperature, followed by 12 µg ml^{-1} rabbit polyclonal anti-*E. histolytica* Gal/GalNAc lectin antibody × 30 min at room temperature, followed by biotinylated goat anti-rabbit immunoglobin G, ABC working solution and diaminobenzidine (Vector, Burlingame, CA, USA) as per the manufacturer's instructions. The identical protocol without Gal/GalNAc lectin was performed as control.

Genotyping

Genomic DNA was isolated from the tails and livers of mice by using the standard phenol/chloroform extraction and ethanol precipitation method. A total of 150 markers with 32 microsatellites and 118 single nucleotide polymorphisms, distinguishing B6 from CBA strain and covering all 19 autosomes and the X chromosome, were used to identify which of the two parental strains contributed to alleles at a specific locus of each N_2 mouse (Table 1). Parental and F_1 DNA served as control for each marker. The linkage maps and marker positions reported were determined using our own data and Map Manager.

Epithelial microarrays

Affymetrix gene chip analysis was performed according to the manufacturer's instructions using murine MOE430 2.0 arrays. Full public access to the raw data is available at https://genes.med.virginia.edu/public_data/index.cgi under 'Eric_Houpt_CBAvsB6naive'. Information about a microrarray experiment (www.mged.org/miame) includes the following. Ceca were obtained from male 6-week-old CBA/J and B6 mice ($n = 3$ each). Cecal contents were rinsed in sterile PBS and the cecal wall was scored, and serosal and muscularis layers were removed. Mucosal epithelial tissues were then placed in RNAlater (Ambion, Austin, TX, USA), homogenized and total RNA extracted using the RNAEasy kit (Qiagen, Valencia, CA, USA). Ribosomal peaks were intact and showed no